iScience

CellPress
OPEN ACCESS

Article

Trans-omic Analysis Reveals ROS-Dependent Pentose Phosphate Pathway Activation after High-Frequency Electrical Stimulation in C2C12 Myotubes

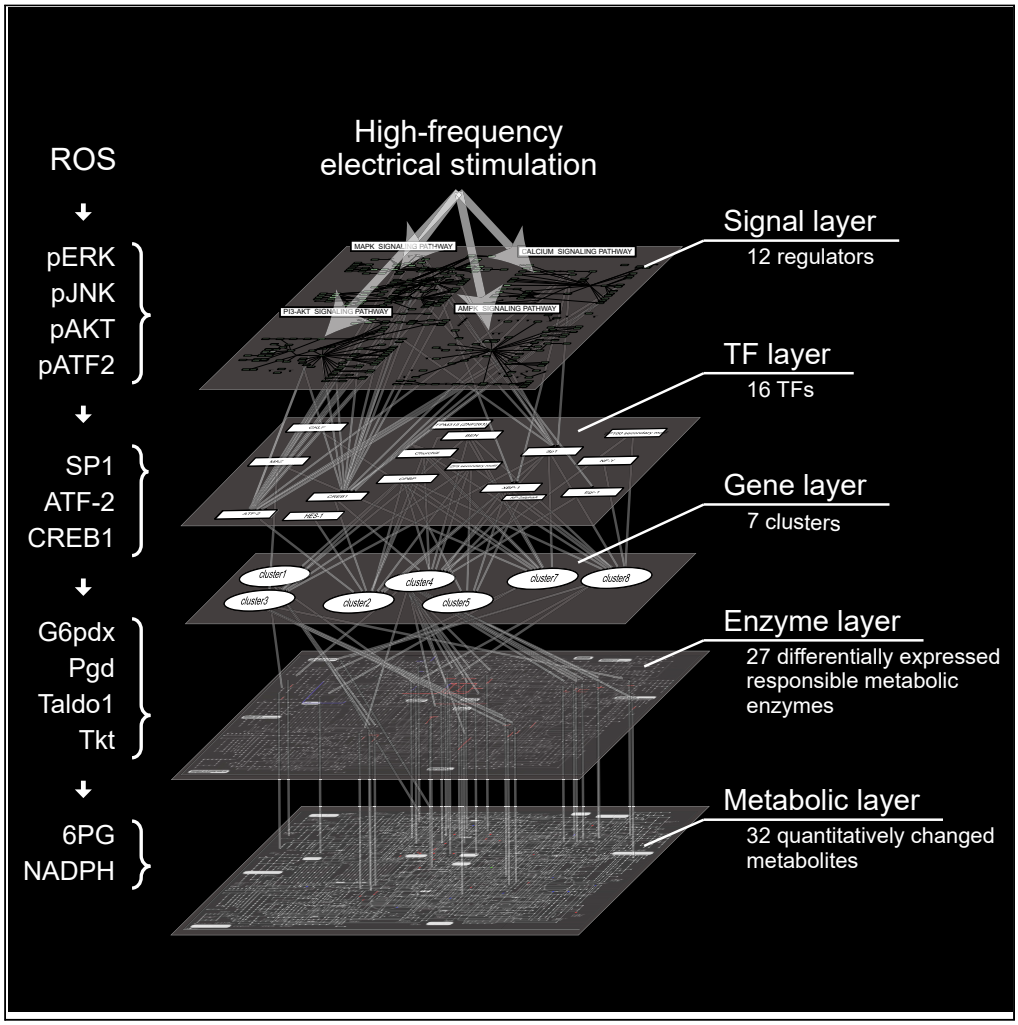

Daisuke Hoshino, Kentaro Kawata, Katsuyuki Kunida, ..., Nobuharu L. Fujii, Tomoyoshi Soga, Shinya Kuroda

skuroda@bs.s.u-tokyo.ac.jp

HIGHLIGHTS

We performed electrical pulse stimulation in differentiated C2C12 myotubes

We constructed trans-omic network after high-frequency electrical pulse stimulation

Trans-omic network integrates metabolome, transcriptome, and signaling molecules

We identified ROS-dependent pentose phosphate pathway activation

Hoshino et al., iScience *23*, 101558
October 23, 2020
https://doi.org/10.1016/j.isci.2020.101558

iScience

CellPress
OPEN ACCESS

Article

Trans-omic Analysis Reveals ROS-Dependent Pentose Phosphate Pathway Activation after High-Frequency Electrical Stimulation in C2C12 Myotubes

Daisuke Hoshino,[1,2] Kentaro Kawata,[1,3] Katsuyuki Kunida,[1,4] Atsushi Hatano,[1,5] Katsuyuki Yugi,[1,6,7,13] Takumi Wada,[1] Masashi Fujii,[8] Takanori Sano,[9] Yuki Ito,[10] Yasuro Furuichi,[11] Yasuko Manabe,[11] Yutaka Suzuki,[10] Nobuharu L. Fujii,[11] Tomoyoshi Soga,[12] and Shinya Kuroda[1,10,14,15,*]

SUMMARY

Skeletal muscle adaptation is mediated by cooperative regulation of metabolism, signal transduction, and gene expression. However, the global regulatory mechanism remains unclear. To address this issue, we performed electrical pulse stimulation (EPS) in differentiated C2C12 myotubes at low and high frequency, carried out metabolome and transcriptome analyses, and investigated phosphorylation status of signaling molecules. EPS triggered extensive and specific changes in metabolites, signaling phosphorylation, and gene expression during and after EPS in a frequency-dependent manner. We constructed trans-omic network by integrating these data and found selective activation of the pentose phosphate pathway including metabolites, upstream signaling molecules, and gene expression of metabolic enzymes after high-frequency EPS. We experimentally validated that activation of these molecules after high-frequency EPS was dependent on reactive oxygen species (ROS). Thus, the trans-omic analysis revealed ROS-dependent activation in signal transduction, metabolome, and transcriptome after high-frequency EPS in C2C12 myotubes, shedding light on possible mechanisms of muscle adaptation.

INTRODUCTION

Physiological muscle adaptation, such as muscle hypertrophy that is characteristic of increases in metabolic enzymes and mitochondrial contents and changes in muscle fiber composition, occurs with continuous exercise and frequent muscle contraction. This adaptation is mediated by cooperative regulation of multiple biological processes, including metabolism, signal transduction, and gene expression (Egan and Zierath, 2013; Hawley et al., 2014). Muscle contraction activates glycolysis and mitochondrial oxidation to maintain energy metabolism. Muscle contraction also activates signaling molecules such as AMP-activated protein kinase (AMPK), Ca^{2+}/calmodulin-dependent protein kinase II (CaMKII), mitogen-activated protein kinases (MAPKs), and mammalian target of rapamycin (mTOR) by changing creatine/phosphocreatine, NAD/NADH, AMP/ATP, Ca^{2+}, reactive oxygen species (ROS), and mechanical stress. Activation of signaling molecules further induces gene expression via transcription factors (TFs). Therefore, skeletal muscle contraction elicits cooperative changes across a multi-layer network, including metabolism, signal transduction, and gene expression, leading to muscle adaptation.

Changes in metabolites, signaling molecule activities, and gene expression in response to muscle contraction depend on the intensity of muscle contraction. In high-intensity exercise, the energy supply by glycogen is dominant and lactate concentration increases, because of activation of glycolysis and glycogenolysis, whereas in low-intensity exercise, the energy supply from fatty acids is dominant and the glycolysis and glycogenolysis rates decrease (van Loon et al., 2001; Romijn et al., 1993). Activation of signaling molecules such as AMPK, p38, and CaMKII also depends on the intensity of muscle contraction (Chen et al., 2003; Egan et al., 2010). Intensity of contraction in the isolated intact muscles is controlled by frequency of electrical stimulation (Cairns et al., 2007). Activation of signaling molecules dependent on frequency of electrical stimulation has thus far been studied using excised muscles and primary myotubes (Atherton et al., 2005; Scheler et al., 2013). Moreover, metabolism-related gene expression is regulated by contraction intensity (Egan et al., 2010; Hildebrandt et al., 2003).

[1]Department of Biological Sciences, Graduate School of Science, University of Tokyo, 7-3-1 Hongo, Bunkyo-ku, Tokyo 113-0033, Japan

[2]Bioscience and Technology Program, Department of Engineering Science, University of Electro-Communications, Tokyo 182-8585, Japan

[3]Isotope Science Center, The University of Tokyo, 2-11-16 Yayoi, Bunkyo-ku, Tokyo 113-0032, Japan

[4]Graduate School of Biological Sciences, and Data Science Center, Nara Institute of Science and Technology, 8916-5 Takayama, Ikoma, Nara 630-0192, Japan

[5]Department of Omics and Systems Biology, Niigata University Graduate School of Medical and Dental Sciences, Niigata, Japan

[6]Laboratory for Integrated Cellular Systems, RIKEN Center for Integrative Medical Science, 1-7-22 Suehiro-cho, Tsurumi-ku, Yokohama, Kanagawa 230-0045, Japan

[7]Institute for Advanced Biosciences, Keio University, Fujisawa, 252-8520, Japan

[8]Department of Mathematical and Life Sciences, Graduate School of Integrated Sciences for Life, Hiroshima University, 1-3-1 Kagamiyama, Higashi-Hiroshima City, Hiroshima 739-8526, Japan

[9]Department of Mechanical and Biofunctional Systems, Institute of Industrial Science, The University of Tokyo, 4-6-1 Komaba, Meguro-ku, Tokyo 153-8505, Japan

[10]Department of Computational Biology and

Continued

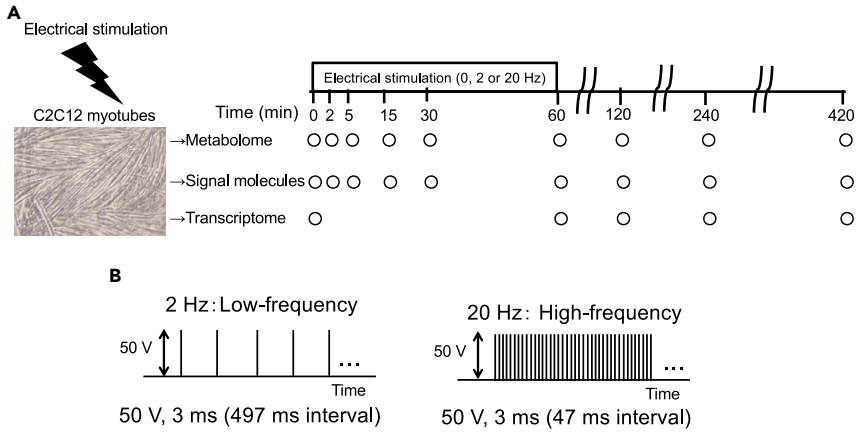

Figure 1. Experimental Design of Metabolome, Signaling Molecules, and Transcriptome Analyses in EPS-Stimulated Differentiated C2C12 Myotubes

(A) Metabolome, signaling molecules, and transcriptome were measured during (0, 2, 5, 15, 30, and 60 min) and after (120, 240, and 420 min) electrical pulse stimulation (EPS) at 0, 2, and 20 Hz in differentiated C2C12 myotubes.

(B) Stimulation protocol of EPS.

Muscle contraction-induced changes in signal transduction, gene expression, and metabolism have been reported to last for hours to days in animals and humans (Chen et al., 2002; Mahoney et al., 2008; Neubauer et al., 2014). Genes induced by muscle contraction, especially those related to energy metabolism, are responsible for long-term effects of exercise such as increase in protein levels of metabolic enzymes and improvement in exercise capacity (Egan and Zierath, 2013; Perry et al., 2010). Metabolites of glycolysis and amino acids change during exercise (Gibala et al., 1997), whereas amino acids and fatty acids in the blood continue to increase for hours after exercise (Peake et al., 2014). Signaling molecules such as phosphorylated Akt (pAkt), mTOR, and S6K also continue to increase after exercise in human skeletal muscle (Camera et al., 2010). However, the interplay among signaling molecules, gene expression, and metabolites after muscle contraction remains to be elucidated.

Quantitative and global measurements using single-omic technology are becoming more available. Metabolome (Miyamoto et al., 2013; Peake et al., 2014), transcriptome (Chen et al., 2002; Mahoney et al., 2008; Neubauer et al., 2014), and phosphoproteome (Camera et al., 2017; Hoffman et al., 2015) have been used to examine the biological mechanisms of exercise in skeletal muscle of rodents and humans. However, despite the progress of single-omic studies, the interplay between different omic layers during exercise has not been reported. Here, we propose using "trans-omics" to construct biochemical interaction networks from multiple omic datasets (Yugi et al., 2016). In our previous studies, we developed a method to construct trans-omic network from several omic datasets and found a novel insulin action for metabolic regulation in hepatoma cells (Kawata et al., 2018; Yugi et al., 2014). However, a trans-omic analysis for muscle contraction has not been explored thus far.

In this study, we performed metabolome and transcriptome analyses and investigated phosphorylation status of signaling molecules in C2C12 myotubes during and after high- or low-frequency electrical pulse stimulation (EPS). We found that extensive changes in metabolites, gene expression, and phosphorylation of signaling molecules selectively occur after high-frequency EPS. We constructed the trans-omic network across signaling molecules, TFs, gene expression, metabolic enzymes, and metabolites induced by high-frequency EPS. The trans-omic analysis revealed that the signaling molecules, gene expression, and metabolites involved in the pentose phosphate pathway increased in a ROS-dependent manner.

RESULTS

Analysis of Metabolome, Signaling Molecules, and Transcriptome Induced by EPS

We performed low- and high-frequency EPS on C2C12 myotubes for 60 min (Manabe et al., 2012) and measured metabolome, signaling molecules, and transcriptome during and after EPS (Figures 1A and 1B).

Medical Sciences, Graduate School of Frontier Sciences, The University of Tokyo, 5-1-5 Kashiwanoha, Kashiwa, Chiba 277-8562, Japan

[11]Department of Health Promotion Sciences, Graduate School of Human Health Sciences, Tokyo Metropolitan University, 1-1 Minami-Osawa, Hachioji, Tokyo 192-0397, Japan

[12]Institute for Advanced Biosciences, Keio University, 246-2 Mizukami, Kakuganji, Tsuruoka, Yamagata 997-0052, Japan

[13]PRESTO, Japan Science and Technology Agency, 1-7-22 Suehiro-cho, Tsurumi-ku, Yokohama, Kanagawa 230-0045, Japan

[14]Core Research for Evolutional Science and Technology (CREST), Japan Science and Technology Agency, Bunkyo-ku, Tokyo 113-0033, Japan

[15]Lead Contact

*Correspondence: skuroda@bs.s.u-tokyo.ac.jp

https://doi.org/10.1016/j.isci.2020.101558

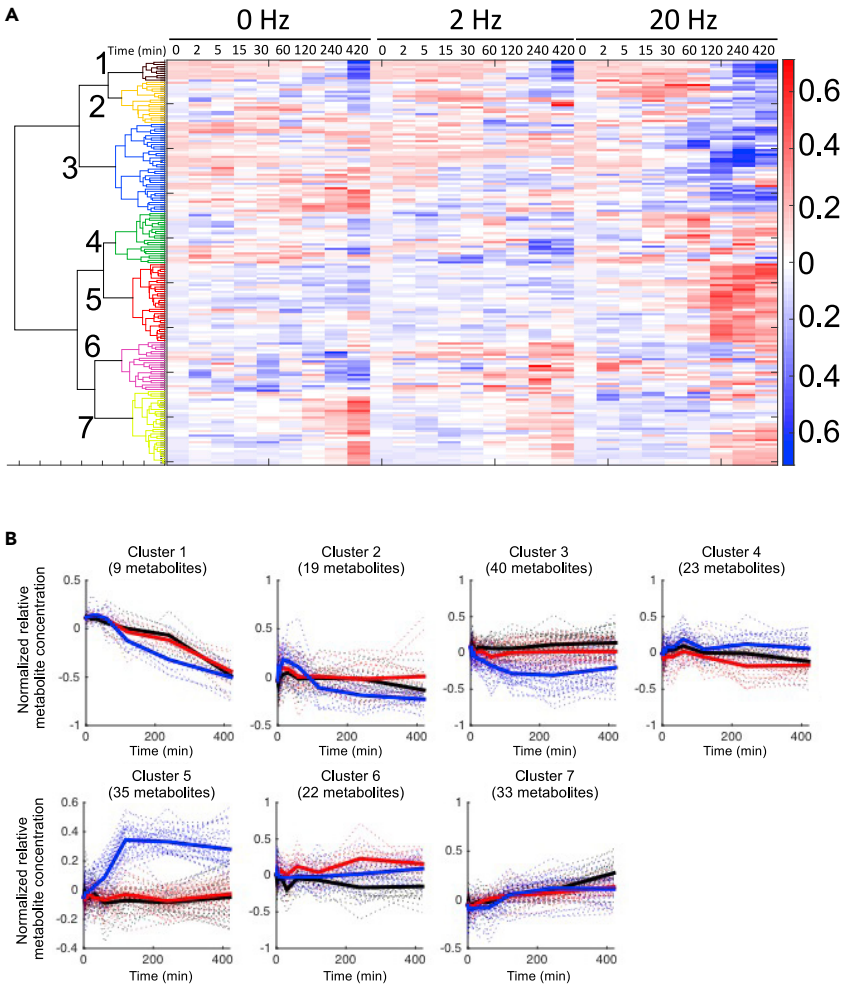

Figure 2. Hierarchal Clustering Analysis of Metabolomic Time Series Data

(A) Heatmap of changes in metabolite concentration at each time point during and after 0, 2, and 20-Hz EPS. Hierarchical clustering was performed using Ward's method with the normalized average value of each metabolite concentration. This average value was calculated with data from three biological replicates.

See also Figure S1 and Table S1.

(B) Time course of metabolites in each cluster. Dashed lines indicate the time series of each metabolite. Black, red, and blue lines indicate values during and after 0, 2, and 20-Hz EPS, respectively. Bold line represents the average value at each condition in each cluster.

For metabolome, 179 metabolites were detected at more than one time point. The metabolites were grouped into seven clusters by cluster analysis using the time series data (Figures 2A, 2B, and S1 and Table S1). The metabolites involved in carbohydrate metabolism, glycolysis, and pentose phosphate pathway were in cluster 5, which showed continuous increase after 20-Hz EPS. Metabolites in TCA cycle (malate, fumarate, and succinate) and nucleotide metabolism (AMP, adenosine, UTP, UDP, and guanosine) were in cluster 2, which showed transient increase during 20-Hz EPS and then returned to the basal level after the EPS. Metabolites in amino acid metabolism were in cluster 3, which showed continuous decrease after 20-Hz EPS. Next, we examined the metabolites that significantly changed with EPS. One single metabolite (6PG) significantly changed during 20-Hz EPS (0–60 min), and 32 metabolites significantly changed after 20-Hz EPS but not during or after 2-Hz EPS (Table S2). These results indicate that extensive metabolic changes occurred after 20-Hz EPS. Among 32 significantly changed metabolites, 17 metabolites increased, 14 metabolites decreased, and one metabolite increased and decreased. G6P, F6P, F1, 6P, DHAP, 3PG, and PEP in glycolysis and 6PG, Ru5P, and R5P in pentose phosphate pathway increased significantly after 20-Hz EPS (Figure 3). UDP-glucose, reduced/oxidized glutathione, and 2-oxoglutarate significantly

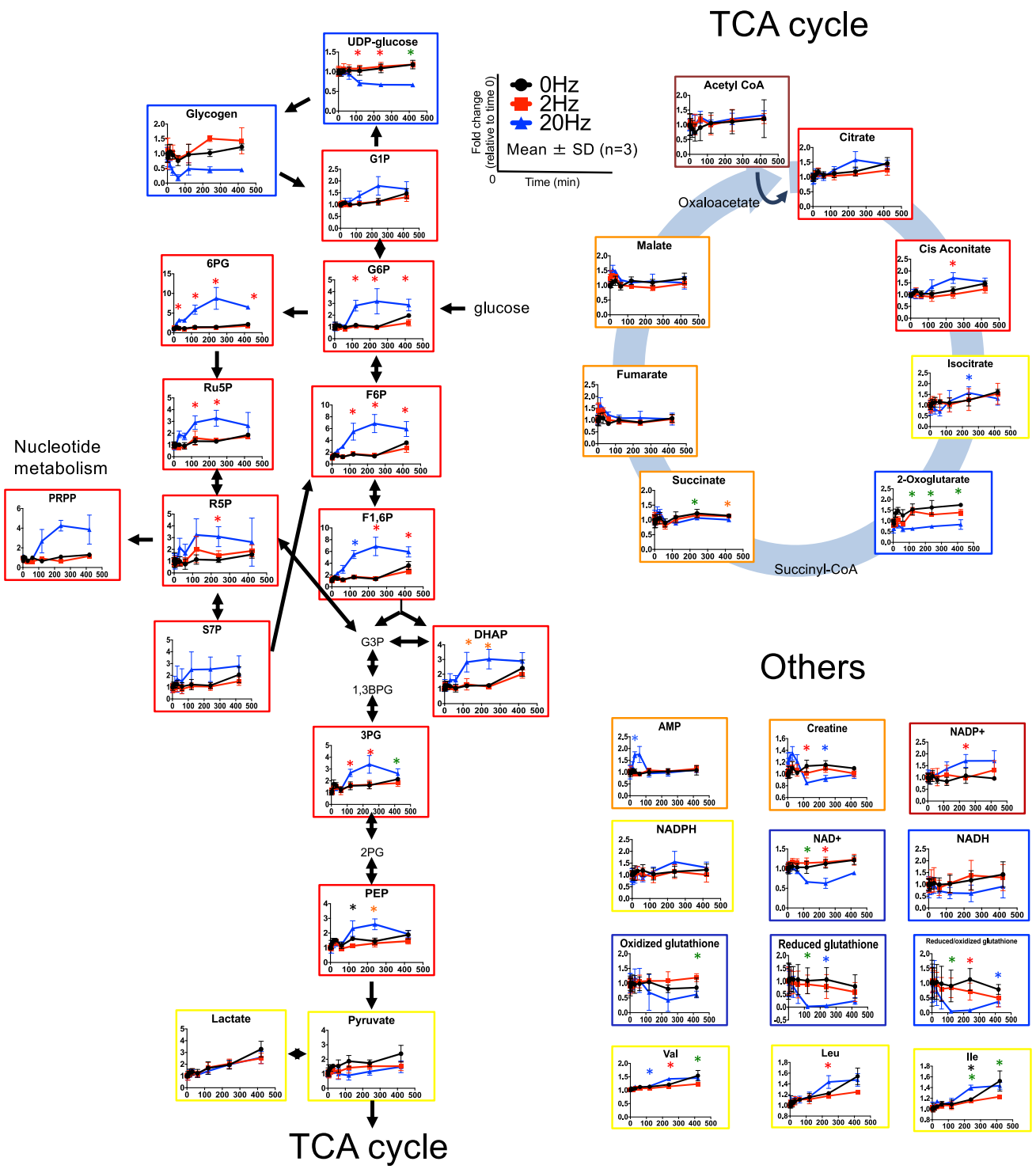

Figure 3. Time Course of Metabolites in Central Carbon Metabolism

Black, red, and blue lines represent 0, 2, and 20 Hz, respectively. Orange, blue, red, and yellow frames correspond to clusters 2, 3, 5, and 7 in Figure 2, respectively. Average concentrations were compared between different stimulations at each time point using the Welch's t test with the Storey's multiple testing correction. At time points where FDR $q < 0.2$, *red indicates significant difference between 0 and 20 Hz and 2 and 20 Hz, *blue indicates significant difference between 0 and 20 Hz, *green indicates significant difference between 2 and 20 Hz, and *black indicates significant difference between 0 and 2 Hz. The means and SDs of three independent experiments each with three biological replicates are shown.

See also Figures S1 and S2 and Table S2.

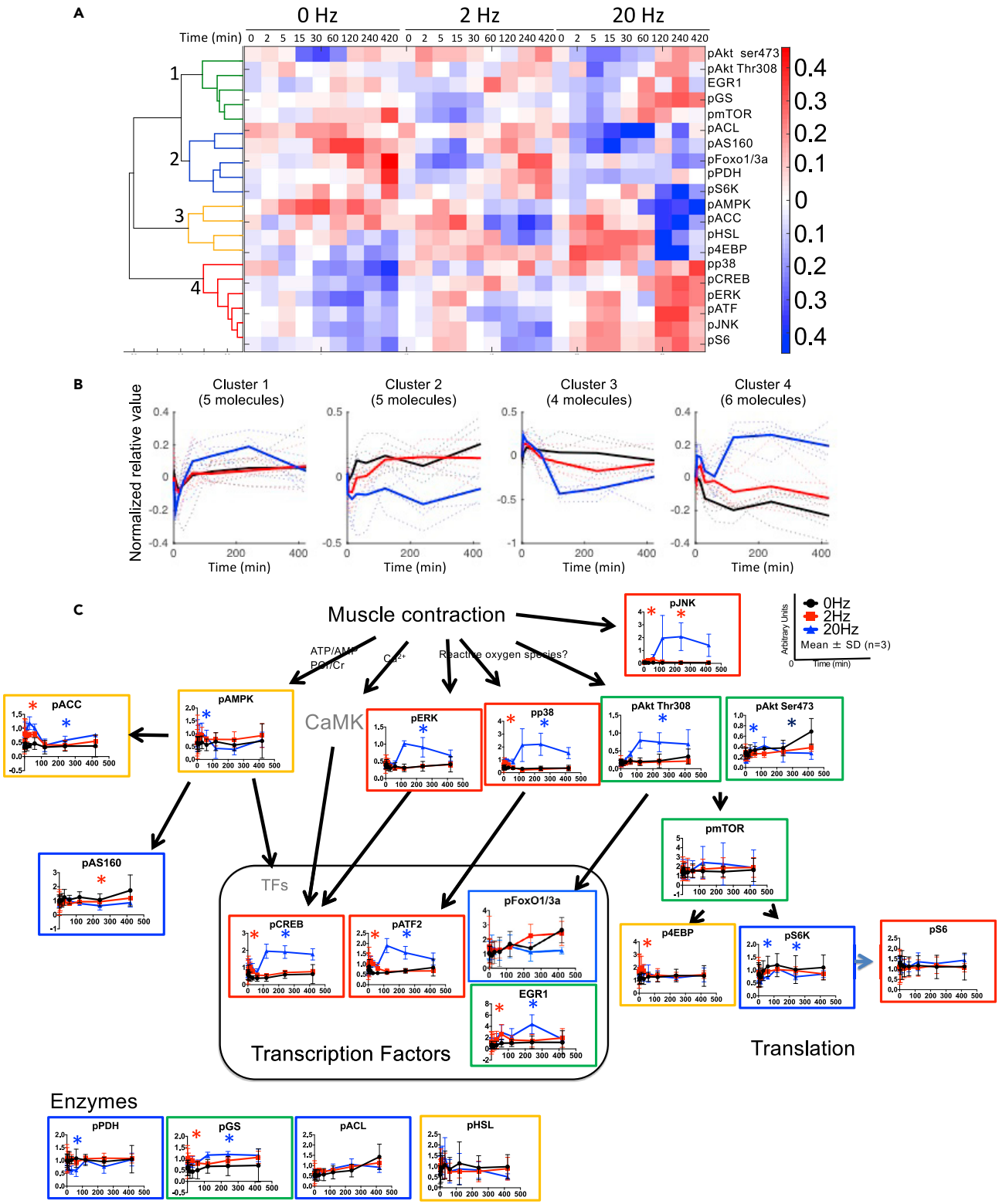

Figure 4. Hierarchal Clustering Analysis Using Time Series Data of Signaling Molecules

(A) Heatmap of changes in signaling molecules at each time point during and after 0, 2, and 20-Hz EPS. Hierarchical clustering was performed using the Ward's method with the normalized average value of each signaling molecule. This average value was calculated with data from three biological replicates.

Figure 4. *Continued*

(B) Time course of signaling molecules in each cluster. Dashed lines indicate the value of each signaling molecule. Black, red, and blue lines indicate values during and after 0, 2, and 20-Hz EPS, respectively. Bold line represents the average value at each EPS frequency in each cluster.

(C) Time course of signaling molecules. Black, red, and blue lines represent 0, 2, and 20 Hz, respectively. Green, blue, yellow, and red frames indicate clusters 1, 2, 3, and 4, respectively. Statistical comparison of the level of each molecule among 0, 2, and 20 Hz at each time point was performed using two-way ANOVA. The calculated p value for the electrical stimulation was corrected for multiple testing using the Benjamini-Hochberg method. FDR $q < 0.1$ was regarded as a significant difference. *Red indicates significant difference between 0 and 20 Hz and 0 and 2 Hz, *blue indicates significant difference between 0 and 20 Hz, and *black indicates the difference between 0 and 2 Hz. The means and SDs of three independent experiments each with three biological replicates are shown.

See also Figure S3 and Table S3.

decreased after 20-Hz EPS. We confirmed that Ca^{2+} signals were induced by 2- and 20-Hz EPS but the Ca^{2+} signals were not maintained during 60 min of 20-Hz EPS. At the same time, the number of myotubes were not reduced (Figure S2A) and ATP did not change significantly after 20-Hz EPS (Figure S2B). Calculated energy charge, an index of energy status of biological cells, showed a slight decrease owing to the changes in ADP (Figure S2C) and AMP levels during 20-Hz EPS and then returned to the basal level after the 20-Hz EPS (Figure S2D). In summary, many metabolites changed only after 20-Hz EPS but not during 20-Hz EPS, and no metabolites changed significantly during or after 2-Hz EPS.

We measured protein levels of phosphorylated signaling molecules, including TFs, protein kinases, and metabolic enzymes, which are known to be regulated by muscle contraction (Egan and Zierath, 2013), using western blot analysis (Figure S3). We performed cluster analysis that resulted in four clusters (Figures 4A–4C and Table S3). pAkt (Ser308 and Thr473), phosphorylated mammalian target of rapamycin (pmTOR), and early growth response protein 1 (EGR1) were in cluster 1, which showed an increase after 60 min of 20-Hz EPS. Phosphorylated pyruvate dehydrogenase (pPDH), phosphorylated ATP citrate lyase (pACL), and phosphorylated S6K (pS6K) were in cluster 2, which showed decrease during and after 20-Hz EPS. Phosphorylated AMPK (pAMPK) and phosphorylated acetyl-CoA carboxylase (pACC) were in cluster 3, which showed a transient increase during 2- and 20-Hz EPS. MAPK such as phosphorylated p38 (pp38), phosphorylated ERK1/2 (pERK), phosphorylated JNK (pJNK), and TFs such as phosphorylated cAMP response element-binding protein (pCREB) and phosphorylated activating TF 2 (pATF2) were in cluster 4, which showed an increase during 2- and 20-Hz EPS and increased after 20-Hz EPS but not after 2-Hz EPS. pERK, p38, JNK, pAkt, pATF2, and pCREB increased significantly after 20-Hz EPS. These results indicate that phosphorylation of a subset of signaling molecules, such as MAPKs and Akt, and TFs, such as pCREB and pATF2, increased continuously after 20-Hz EPS.

We performed mRNA sequencing of the myotubes, mapped the sequences to the mouse genome using TopHat (Trapnell et al., 2009), and calculated mRNA expression level as fragments per kilobase of exon per million fragments mapped (FPKM) using Cufflinks (Trapnell et al., 2010). We thus obtained expression data of 11,185 genes throughout the time course (Figure S4). To identify differentially expressed genes (DEGs) in response to EPS, we calculated fold-change of FPKMs at each time point compared with those at time 0 at 2- and 20-Hz EPS and defined genes with changes of 2.0-fold or more and of 0.5-fold or less as DEGs. We identified 800 DEGs. To clarify the pattern of time-dependent changes of the DEGs, we performed hierarchical cluster analysis using the time series data of the DEGs and obtained eight clusters (Figure 5). Next, we examined biological functions of genes in each cluster using KEGG pathway analysis in the DAVID online tool (Huang et al., 2008, Table S4). Genes in MAPK and p53 signaling pathways were enriched in cluster 2, and genes in glutathione metabolism and pentose phosphate pathway were enriched in cluster 4. Clusters 2 and 4 showed continuous increase after 20-Hz EPS. Genes in phosphatidylinositol signaling were enriched in cluster 5, and genes in focal adhesion and TGF-beta signaling pathways were enriched in cluster 7. The clusters 5 and 7 showed continuous decrease after 20-Hz EPS. Taken together, there were widespread and persistent changes in metabolite, phosphorylation of signaling molecules, and gene expression after 20-Hz EPS.

Connection of the Transcriptomic Layer to the Signaling Layer

Having observed changes in both phosphorylation of signaling molecules and gene expression after 20-Hz EPS, we set out to identify TFs that connect these two layers. The analysis was conducted in two steps: (1) prediction of TFs and (2) identification of signaling molecules regulating the predicted TFs using KEGG database.

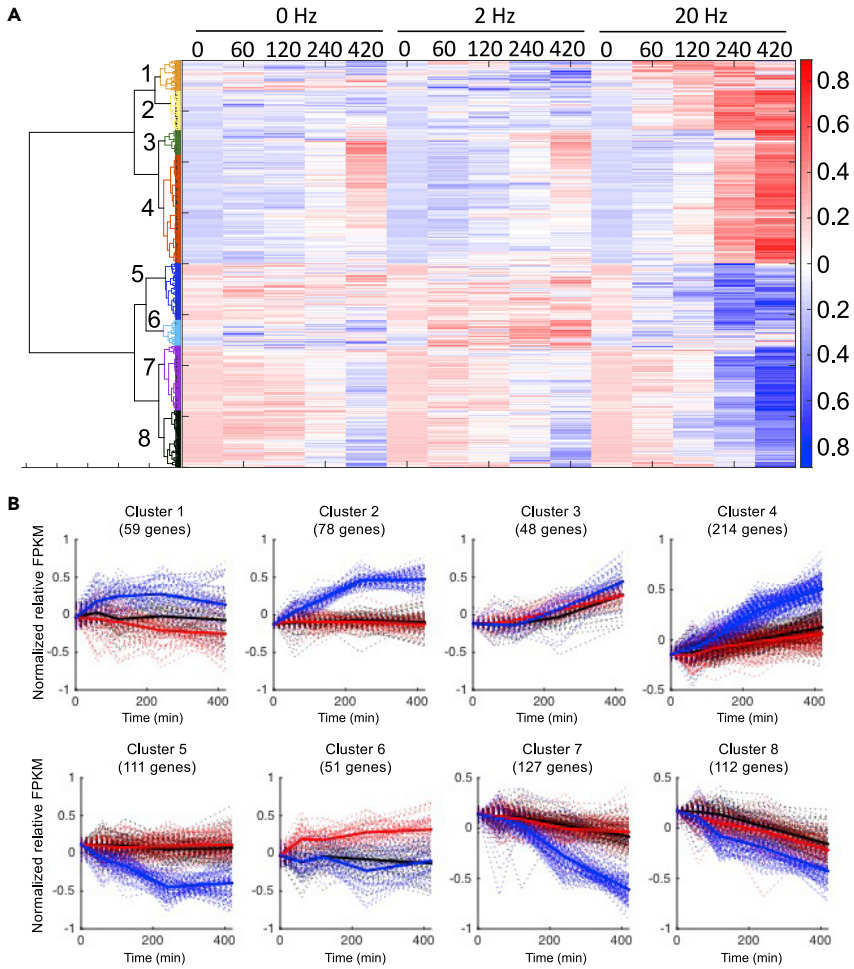

Figure 5. Hierarchal Clustering Analysis Using Time Series of DEGs from Transcriptomic Data

(A) Heatmap of changes in DEGs at each time point during and after 0, 2, and 20-Hz EPS. Hierarchical clustering was performed using Ward's method with normalized value of each DEG (one independent biological experiment at each time point).

(B) Time course of DEGs in each cluster. Dashed lines indicate the time series of each DEG. Black, red, and blue lines indicate values during and after 0, 2, and 20-Hz EPS. Bold line represents the average value at each EPS frequency in each cluster.

See also Figure S4 and Tables S4–S7.

To identify TFs that regulate DEGs, we identified putative binding motifs for TFs in the promoter region of each DEG (−300 bp to +100 bp around the consensus transcription start site [Arner et al., 2015; Kinsella et al., 2011]) using TRANSFAC (Matys et al., 2006) and Match (Kawata et al., 2018; Kel et al., 2003). Subsequently, we used a modified motif enrichment analysis to predict TFs that bind to promoters of DEGs in each cluster (Mina et al., 2015). We thus predicted 16 TFs for the DEG clusters (Figure 6), with some of them shared by multiple clusters.

Next, we identified the signaling molecules that regulate these predicted TFs, using KEGG pathway analysis. We focused on MAPK, PI3K-Akt, AMPK, and calcium signaling pathways (Figure S5), which are known to be regulated by muscle contraction (Egan and Zierath, 2013). Twelve signaling molecules were identified as the regulators of the predicted TFs: Akt, ERK, PKA, PKC, JNK, p38, mTORC2, MSK1/2, CAMK, GSK3, CREB, and EGR1. Among them, phosphorylation of ERK, Akt, CREB, JNK, p38, and EGR1 increased significantly after 20-Hz EPS (Figure 4C). These results indicate that the signaling molecules upstream of TFs and their target DEGs are activated after 20-Hz EPS.

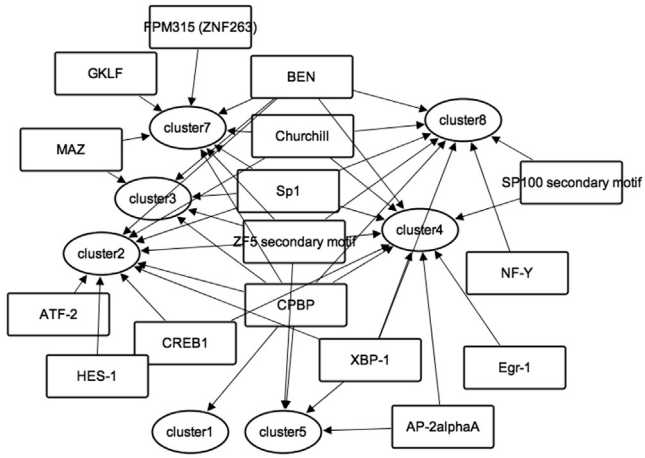

Figure 6. Prediction of Transcription Factors from Clusters of DEGs Using Motif Enrichment Analysis

Squares indicate predicted TFs. Circles indicate clusters resulting from hierarchical clustering. Arrows indicate from which cluster the TF was predicted.

See also Figure S4.

Connection of the Transcriptomic Layer to the Metabolic Layer

We connected the metabolomic layer with the transcriptomic layer by identifying metabolic enzymes responsible for the changes in the metabolites. We identified responsible metabolic enzymes using the method developed in our previous study (Yugi et al., 2014). First, we measured levels of 32 metabolites that significantly changed after 20-Hz EPS. Second, we searched for metabolic enzymes that have these 32 metabolites as substrates or products using KEGG database. Third, the metabolic enzymes encoded by DEGs were defined as responsible metabolic enzymes. As a result, 27 responsible metabolic enzymes were identified (Table S5). KEGG pathway enrichment analysis showed that the 27 responsible metabolic enzymes are involved in carbon metabolism, pentose phosphate pathway, and biosynthesis of amino acids (Table S6). Given that 27 metabolic enzymes were encoded by DEGs in cluster 4 in Figure 5, which continuously increased after 20 Hz, we performed KEGG pathway enrichment analysis for cluster 4. Among enzymes involved in central carbon metabolism, genes encoding metabolic enzymes in the pentose phosphate pathway were the largest gene group that was significantly enriched (Table S7). These results indicate that both the metabolites and the genes encoding the metabolic enzymes in the pentose phosphate pathway increased after 20 Hz stimulation (Figure S6).

Construction of the Trans-omic Network Induced by EPS

Our analysis showed that, after 20-Hz EPS, extensive changes occur in multiple layers of metabolites, signal molecules, and gene expression. Therefore, we constructed a trans-omic network of metabolites, metabolic enzymes, gene expression, TFs, and signal molecules after 20-Hz EPS (Figure 7). Thirty-two metabolites significantly changed after 20-Hz EPS. Twenty-seven DEGs encoding metabolic enzymes use these 32 metabolites as substrates or products. We performed hierarchical clustering analysis using 800 DEGs and predicted 16 TFs for the DEG clusters. Twelve signaling molecules presumably interact with these 16 TFs, as they are involved in the same KEGG pathways (MAPK, AMPK, calcium, and PI3K-Akt pathways).

ROS-Dependent Metabolic Network after High-Frequency EPS

We found that ROS were involved in the multi-layer responses after 20-Hz EPS because our results showed that reduced/oxidized glutathione, which is a marker for accumulation of ROS, greatly and continuously changed after 20-Hz stimulation (Figure 3A and Table S2). Consistently, p38 and JNK phosphorylation, which are known to be regulated by ROS, increased after 20-Hz EPS (Figure 4C). To experimentally validate our findings, we added an antioxidant, N-acetylcysteine (NAC), immediately after 1 h of 20-Hz EPS and examined changes of signaling molecules and metabolites 180 min time point after of the 1 h 20-Hz EPS. The addition of NAC attenuated the changes in reduced/oxidized glutathione after 20-Hz EPS. The addition of NAC after 20-Hz EPS also suppressed phosphorylation of JNK, ERK, Akt Ser308, and ATF2 after 20-Hz EPS (Figure 8A) and the increase of 6PG, S7P, and NADPH in the pentose phosphate pathway

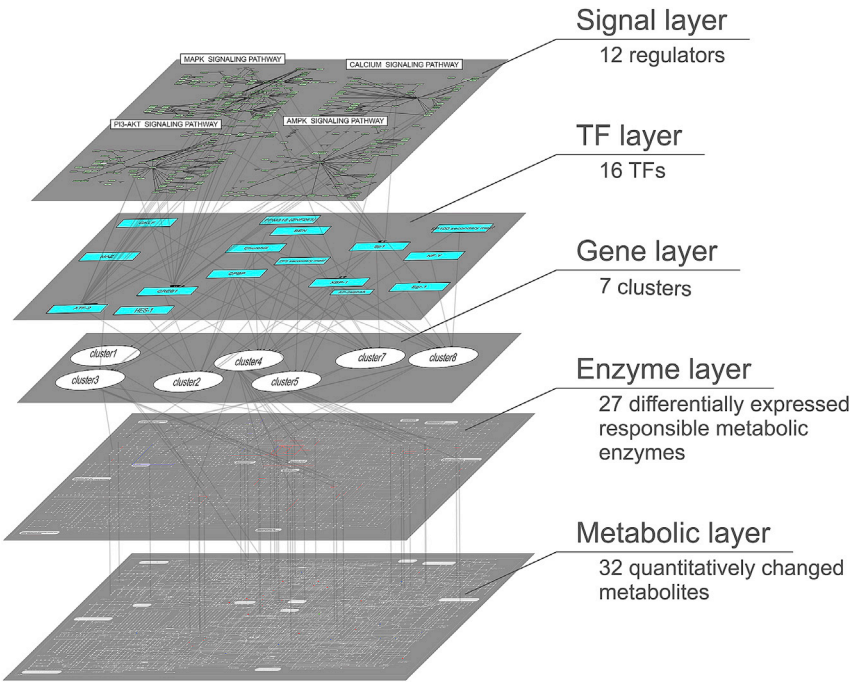

Figure 7. Trans-omic Network after High-Frequency Electrical Stimulation of C2C12 Myotubes

The diagram connects five layers of signaling molecules, transcriptional factors, gene expression, metabolic enzymes, and metabolites. In the signaling molecules layer, the 12 regulators were identified in the four KEGG signaling pathways and were shown in red, and the others were shown in green. In the transcriptional factor and gene expression layers, the 16 TFs were predicted from seven clusters of DEGs. In the metabolic enzyme layer, 27 differentially expressed responsible metabolic enzymes were identified, and in the metabolite layer, 32 metabolites were identified as quantitatively changed metabolites.

See also Figures S5 and S6 and Tables S5–S7.

(Figure 8B). These results indicate the pivotal role of ROS in inducing changes of signal molecules and metabolites involved with the pentose phosphate pathway after 20-Hz EPS (Figure 8C).

DISCUSSION

In this study, we characterized metabolome, transcriptome, and phosphorylation and protein of signal molecules in the EPS-stimulated C2C12 myotubes and constructed a trans-omic network by integrating the multi-omic data. The trans-omic analysis and experimental validation revealed that ROS-mediated phosphorylation of signaling molecules, gene expression of metabolic enzymes, and metabolites in the pentose phosphate pathway were upregulated after 20-Hz EPS.

In this study, we used an electrical stimulation system for C2C12 myotubes to that has been shown to mimic muscle contraction *in vitro* in our laboratory (Furuichi et al., 2018; Manabe et al., 2012; Matsuda et al., 2020; Wada et al., 2020). We used 2 Hz for low-frequency and 20 Hz for high-frequency stimulation. Previous studies confirmed that 20 Hz is high frequency for C2C12 myotubes (Fujita et al., 2007; Yamasaki et al., 2009) but 20 Hz is not considered high-frequency stimulation for skeletal muscle contraction *in vivo* (Cairns et al., 2007). Creatine and AMP increased transiently during 20 Hz stimulation, suggesting activation of ATP hydrolysis and PCr breakdown. These results are consistent with electrical stimulated rat skeletal muscles (Spriet, 1989) and exercised human skeletal muscles (Parolin et al., 1999; Perry et al., 2008). However, the increase in ADP and AMP levels of C2C12 by EPS was smaller than that of *in vivo* muscle contraction, suggesting the difference between C2C12 EPS and *in vivo* muscle contraction. In the TCA cycle intermediates, Fumarate and Malate increased and returned to basal rapidly during 20 Hz, and 2-oxoglutarate decreased due to 20-Hz EPS. These results are consistently seen in human skeletal muscles during 60-min exercise (Gibala et al., 1997). In signaling molecules, pACC, pJNK and pp38 increased during 2- and 20-Hz EPS. This result is similar to the previous study using EPS in C2C12 myotubes (Manabe et al., 2012). pERK, pp38,

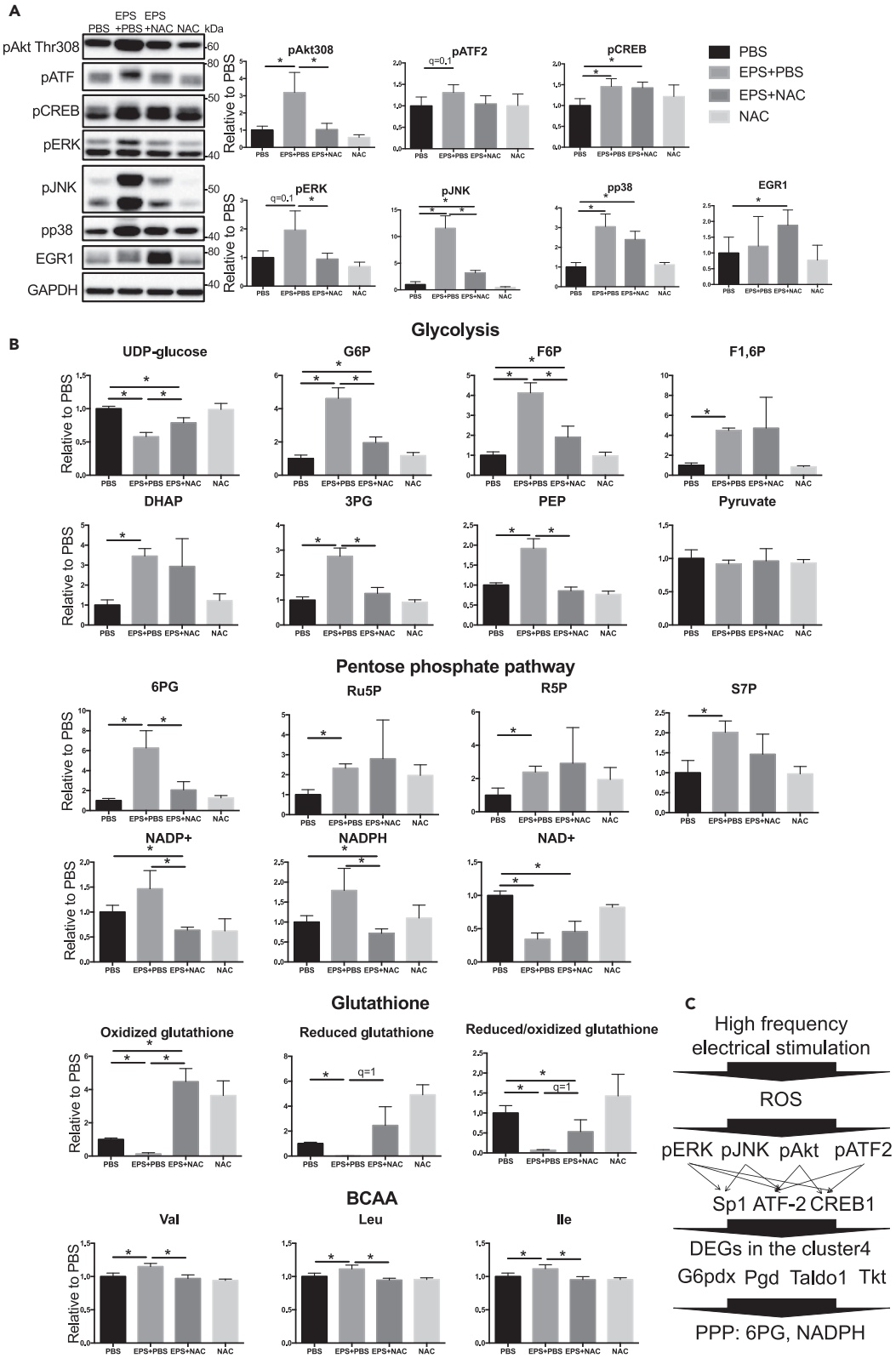
A
EPS EPS
PBS +PBS +NAC NAC kDa
pAkt Thr308
pATF
pCREB
pERK
pJNK
pp38
EGR1
GAPDH
60
80
50
40
50
40
80
40
Relative to PBS
pAkt308
pATF2
pCREB
pERK
pJNK
pp38
EGR1
q=0,1
PBS
EPS+PBS
EPS+NAC
NAC
B
Glycolysis
UDP-glucose
G6P
F6P
F1,6P
DHAP
3PG
PEP
Pyruvate
Pentose phosphate pathway
6PG
Ru5P
R5P
S7P
NADP+
NADPH
NAD+
Glutathione
Oxidized glutathione
Reduced glutathione
Reduced/oxidized glutathione
q=1
BCAA
Val
Leu
Ile
C
High frequency electrical stimulation
ROS
pERK pJNK pAkt pATF2
Sp1 ATF-2 CREB1
DEGs in the cluster4
G6pdx Pgd Taldo1 Tkt
PPP: 6PG, NADPH

Figure 8. Effects of NAC on Signaling Molecules and Metabolites after 20-Hz EPS

(A and B) Signaling molecules and metabolite concentrations. Welch's t test was performed on each signaling molecule and each metabolite, and multiple comparisons were performed based on FDR (BH method). *q < 1 was defined as a significant difference. The means and SDs of four independent experiments each with four biological replicates are shown.

(C) ROS-dependent activation of signaling molecules, enzymes, and metabolites involved with the pentose phosphate pathway (PPP) after high-frequency electrical stimulation.

pJNK, pAkt, pATF2, and pCREB increased continuously after 20-Hz EPS. Previous studies have reported that pAkt and pp38 increased continuously in skeletal muscles after exercise (Camera et al., 2010; Williamson et al., 2006). Gene expression results show that EGR1, IL6, FOS, HSPB1, and mdm2 increased after 20-Hz EPS. These genes were known to increase after exercise or EPS (Furuichi et al., 2018; Irrcher and Hood, 2004; Neubauer et al., 2014; Roudier et al., 2012). Gene expression of dgkq, Pik3r1, PIK3C2B, and Thbs1 decreased after 20-Hz EPS. These reductions after EPS have never been reported but may be important for an increase in insulin sensitivity in skeletal muscles because these genes are associated with insulin resistance (Alliouachene et al., 2015; Inoue et al., 2013; Mannerås-Holm et al., 2015; McCurdy et al., 2012). We confirmed that Ca^{2+} signals were induced by 2- and 20-Hz EPS but these were not maintained during 60 min of 20-Hz EPS. This result suggests fatigue state of myotubes after 60 min of 20-Hz EPS; 20-Hz EPS was considered high-frequency stimulation because Ca^{2+} signal and contraction responses against frequency are different between C2C12 myotubes and skeletal muscle. A sustained increase in Ca^{2+} signal and tetanus contraction by 10-Hz EPS in C2C12 myotubes were shown previously (Fujita et al., 2007; Yamasaki et al., 2009). However, the number of cells and ATP were not reduced during and after 20-Hz EPS. Calculated energy charge reduced slightly during 20 Hz but returned to the basal level after the 20-Hz EPS. We believe that EPS-stimulated biological alterations involved with metabolome, signaling molecules, and gene expression were not attributable to cell death.

Because phosphorylation of signaling molecules in response to ROS and markers for ROS accumulation increased after 20-Hz EPS, we hypothesized that ROS accumulation after 20-Hz EPS is involved in activation of the pentose phosphate pathway. ROS accumulation in muscle by *in vitro* EPS has also been reported in the previous study (Horie et al., 2015). Although phosphorylation of ERK, p38, JNK, Akt, ATF2, and CREB increased significantly after 20-Hz EPS, addition of NAC, an antioxidant, after 20-Hz EPS inhibited phosphorylation of Akt, ERK, and JNK but not the other signaling factors. Previous studies suggest that activation of Akt signaling upregulates expression of genes encoding the metabolic enzymes and corresponding metabolites in the pentose phosphate pathway (Wagle et al., 1998; Wu et al., 2017). ERK and JNK have also been shown to mediate activation of the pentose phosphate pathway in cancer cells (Papa et al., 2019). Since NAC was added after 20-Hz EPS to clarify the effect of ROS accumulation after 20-Hz EPS, ROS production and accumulation during EPS could not be suppressed. It is possible that ROS during 20-Hz EPS affected the activation of signaling molecule. Indeed, EGR1 was not attenuated by NAC. This result may be associated with ROS production and/or accumulation during 20-Hz EPS because EGR1 increased rapidly in C2C12 myotubes after electrical stimulation (Irrcher and Hood, 2004). These results suggest that accumulation of ROS after 20-Hz EPS regulates activation of the pentose phosphate pathway via Akt, ERK, and JNK signaling.

We identified responsible metabolic enzymes, such as Pgd, Tkt, Taldo1, and G6pdx, which are involved in the pentose phosphate pathway, using gene expression data. These metabolic enzymes are encoded by DEGs in cluster 4, which continuously increased after 20-Hz EPS. These results indicate that the pentose phosphate pathway was activated after 20-Hz EPS. To the best of our knowledge, this is the first study reporting that expression levels of genes encoding enzymes of the pentose phosphate pathway increased after high-frequency electrical stimulation. We estimate that gene expression of enzymes related in the pentose phosphate pathway was also inhibited by NAC because phosphorylation of Akt, ERK, and JNK was inhibited. Previous studies reported that these signaling molecules regulate gene expression of enzymes involved in pentose phosphate pathway (Ham et al., 2013; Wang et al., 2019; Wu et al., 2017). Therefore, our data-driven trans-omic analysis revealed activation of the pentose phosphate pathway after high-frequency electrical stimulation.

Along with increase in gene expression related to the pentose phosphate pathway, metabolites in the same pathway, such as Ru5P, 6PG, and R5P, increased significantly after 20-Hz EPS. It has been shown that insulin sensitivity and glucose uptake increased for up to 3 h after muscle contraction (Cartee et al., 1989). Transported glucose has been thought to be used primarily for glycogen repletion (Jentjens and

Jeukendrup, 2003). Flux of glucose into the alternative pathway, the pentose phosphate pathway, has received little attention because expression levels of genes and proteins for the enzymes are relatively low in skeletal muscle (Battistuzzi et al., 1985). Our findings suggest that the pentose phosphate pathway, another glucose metabolic pathway in addition to glycogen synthesis, is also triggered after high-frequency electrical stimulation for physiological adaptation. Furthermore, addition of NAC suppressed the increase in metabolites from the pentose phosphate pathway such as 6PG and NADPH. There are two possible explanations for the ROS-dependent activation of the pentose phosphate pathway. First, ROS is known to enhance insulin sensitivity and glucose uptake (Loh et al., 2009). Alternatively, protein levels of the enzymes involved in the pentose phosphate pathway were increased, although we did not measure protein abundance and protein phosphorylation in large scale in this study.

Interestingly, the concentration of metabolites in the glycolysis pathway was also increased after 20-Hz EPS. It is unclear why the concentrations of these metabolites increased after 20-Hz EPS because the flux of the glycolytic system increases rapidly owing to exercise and decreases rapidly at basal state after exercise (Crowther et al., 2002; Spriet et al., 1985). We estimate that increases in these intermediate metabolites did not reflect an increase in glycolytic flux. The activity of pyruvate kinase may be associated with increases in these metabolite concentrations because the pyruvate did not increase in spite of increasing from G6P to PEP. It is necessary to examine metabolic flux because the concentration is a balance between production and degradation of the metabolite.

The ROS-dependent activation of the pentose phosphate pathway may be associated with physiological adaptation of skeletal muscle. The pentose phosphate pathway plays a role in producing substrates for nucleic acid synthesis and lipid synthesis. Since high-frequency stimulation is accompanied by muscle damage, it is physiologically important that nucleic acid synthesis and lipid synthesis are activated for muscle hypertrophy and membrane recovery. We measured NADPH, which is a source of lipid synthesis, and PRPP, which is a source of nucleic acid synthesis. NADPH and PRPP of 20-Hz EPS at 240 min were about 1.5- and 4-fold, respectively, higher than those of 0-Hz EPS at 240 min, although these differences were not significant. These results suggest the activation of lipid synthesis and nucleotide synthesis after 20-Hz EPS to lead to physiological adaptation. Indeed, it has been shown that regeneration from drug-induced muscle damage requires activation of the pentose phosphate pathway (Wagner et al., 1978). Furthermore, ROS has been shown to be associated with repair of membrane damage after eccentric muscle contraction (Horn et al., 2017). Taken together, our findings of ROS-dependent activation of the pentose phosphate pathway provide new insights into muscle adaptation under physiological conditions.

Limitations of the Study

Trans-omic analysis revealed ROS-dependent pentose phosphate pathway activation after 20-Hz EPS in C2C12 myotubes. We could not construct low-frequency stimulation-induced trans-omic network because of weak responses in each multi-layer in this study. Clarifying the difference in trans-omic network between low-frequency and high-frequency stimulation will further deepen the understanding of mechanisms of frequency-dependent muscle adaptation. Furthermore, it is not clear whether exercise in animals stimulates the signaling molecules, genes, and metabolites in the pentose phosphate pathway *in vivo*. In the future, it is necessary to examine the validation of trans-omic network we constructed and activation of pentose phosphate pathway using an animal experiment. We also could not verify the physiological significance of activation of the pentose phosphate pathway. Exercise has a wide variety of modes such as endurance exercise and resistance exercise; cellular responses are different between each exercise mode (Atherton et al., 2005). Therefore, clarifying the relationship between exercise modes and activation of the pentose phosphate pathway enables clarification of the physiological significance *in vivo*.

Resource Availability

Lead Contact

Further information and requests for resources and reagents should be directed to and will be fulfilled by the Lead Contact, Shinya Kuroda (skuroda@bs.s.u-tokyo.ac.jp).

Materials Availability

This study did not generate new unique reagents.

Data and Code Availability

The RNA-seq data in this study are available at DDBJ (Accession number DRA010400).

METHODS

All methods can be found in the accompanying Transparent Methods supplemental file.

SUPPLEMENTAL INFORMATION

Supplemental Information can be found online at https://doi.org/10.1016/j.isci.2020.101558.

ACKNOWLEDGMENTS

We thank our laboratory members for critically reading this manuscript and for their technical assistance with the experiments. This work was supported by the Creation of Fundamental Technologies for Understanding and Control of Biosystem Dynamics, CREST (JPMJCR12W3) from the Japan Science and Technology Agency (JST) and by the Japan Society for the Promotion of Science (JSPS) KAKENHI Grant Number 17H06299, 17H06300. D.H. received a Grant-in-Aid for JSPS Research Fellow (14J05223). K. Kawata receives funding from JSPS KAKENHI (19K16635) and the Takeda Life Science Foundation. K. Kunida receives funding from a Grant-in-Aid for Young Scientists (B) (16K19028) from JSPS. K.Y. receives funding from the JSPS (KAKENHI grant numbers JP15H05582 and JP18H05431 and Creation of Innovative Technology for Medical Applications Based on the Global Analyses and Regulation of Disease-Related Metabolites) and PRESTO (JPMJPR1538) from the JST. Y.S. was supported by the JSPS KAKENHI Grant Number 17H06306. T. Soga receives funding from the AMED-CREST (JP18gm0710003) from the Japan Agency for Medical Research and Development, AMED.

AUTHOR CONTRIBUTIONS

Conception and design of research: D.H. and S.K. Conception and design of the experiments: D.H., K. Kunida, A.H., K.Y., T.W., Y.F., Y.M., N.L.F., and S.K. Collection, analysis, and interpretation of data: D.H., K. Kawata, K. Kunida, A.H., K.Y., T.W., M.F., T. Sano, Y.I., Y.F., Y.M., Y.S., N.L.F., T. Soga, and S.K. Drafting the article or revising it critically for important intellectual content: D.H., K. Kawata, A.H, Y.K., T.W., and S.K. All authors approved the final version of the manuscript and listed qualify for authorship.

DECLARATION OF INTERESTS

The authors declare no conflicts of interest.

Received: June 10, 2020
Revised: August 6, 2020
Accepted: September 10, 2020
Published: October 23, 2020

REFERENCES

Alliouachene, S., Bilanges, B., Chicanne, G., Anderson, K.E., Pearce, W., Ali, K., Valet, C., Posor, Y., Low, P.C., Chaussade, C., et al. (2015). Inactivation of the class II PI3K-C2β potentiates insulin signaling and sensitivity. Cell Rep. *13*, 1881–1894.

Arner, E., Daub, C.O., Vitting-Seerup, K., Andersson, R., Lilje, B., Drablos, F., Lennartsson, A., Ronnerblad, M., Hrydziuszko, O., Vitezic, M., et al. (2015). Transcribed enhancers lead waves of coordinated transcription in transitioning mammalian cells. Science *347*, 1010–1014.

Atherton, P.J., Babraj, J., Smith, K., Singh, J., Rennie, M.J., and Wackerhage, H. (2005). Selective activation of AMPK-PGC-1alpha or PKB-TSC2-mTOR signaling can explain specific adaptive responses to endurance or resistance training-like electrical muscle stimulation. FASEB J. *19*, 786–788.

Battistuzzi, G., D'Urso, M., Toniolo, D., Persico, G.M., and Luzzatto, L. (1985). Tissue-specific levels of human glucose-6-phosphate dehydrogenase correlate with methylation of specific sites at the 3' end of the gene. Proc. Natl. Acad. Sci. U S A *82*, 1465–1469.

Cairns, S.P., Chin, E.R., and Renaud, J.-M. (2007). Stimulation pulse characteristics and electrode configuration determine site of excitation in isolated mammalian skeletal muscle: implications for fatigue. J. Appl. Physiol. *103*, 359–368.

Camera, D.M., Edge, J., Short, M.J., Hawley, J.A., and Coffey, V.G. (2010). Early time course of akt phosphorylation after endurance and resistance exercise. Med. Sci. Sports Exerc. *42*, 1843–1852.

Camera, D.M., Burniston, J.G., Pogson, M.A., Smiles, W.J., and Hawley, J.A. (2017). Dynamic proteome profiling of individual proteins in human skeletal muscle after a high-fat diet and resistance exercise. FASEB J. *31*, 5478–5494.

Cartee, G.D., Young, D.A., Sleeper, M.D., Zierath, J., Wallberg-Henriksson, H., and Holloszy, J.O. (1989). Prolonged increase in insulin-stimulated glucose transport in muscle after exercise. Am. J. Physiol. *256*, E494–E499.

Chen, Y.-W., Nader, G.A., Baar, K.R., Fedele, M.J., Hoffman, E.P., and Esser, K.A. (2002). Response of rat muscle to acute resistance exercise defined by transcriptional and translational profiling. J. Physiol. *545*, 27–41.

Chen, Z.-P., Stephens, T.J., Murthy, S., Canny, B.J., Hargreaves, M., Witters, L.A., Kemp, B.E., and McConell, G.K. (2003). Effect of exercise intensity on skeletal muscle AMPK signaling in humans. Diabetes *52*, 2205–2212.

Crowther, G.J., Kemper, W.F., Carey, M.F., and Conley, K.E. (2002). Control of glycolysis in contracting skeletal muscle. II. Turning it off. Am. J. Physiol. Endocrinol. Metab. *282*, E74–E79.

Egan, B., and Zierath, J.R. (2013). Exercise metabolism and the molecular regulation of skeletal muscle adaptation. Cell Metab. *17*, 162–184.

Egan, B., Carson, B.P., Garcia-Roves, P.M., Chibalin, A.V., Sarsfield, F.M., Barron, N., McCaffrey, N., Moyna, N.M., Zierath, J.R., and O'Gorman, D.J. (2010). Exercise intensity-dependent regulation of peroxisome proliferator-activated receptor coactivator-1 mRNA abundance is associated with differential activation of upstream signalling kinases in human skeletal muscle. J. Physiol. *588*, 1779–1790.

Fujita, H., Nedachi, T., and Kanzaki, M. (2007). Accelerated de novo sarcomere assembly by electric pulse stimulation in C2C12 myotubes. Exp. Cell Res. *313*, 1853–1865.

Furuichi, Y., Manabe, Y., Takagi, M., Aoki, M., and Fujii, N.L. (2018). Evidence for acute contraction-induced myokine secretion by C2C12 myotubes. PLoS One *13*, e0206146.

Gibala, M.J., Tarnopolsky, M.A., and Graham, T.E. (1997). Tricarboxylic acid cycle intermediates in human muscle at rest and during prolonged cycling. Am. J. Physiol. *272*, E239–E244.

Ham, M., Lee, J.-W., Choi, A.H., Jang, H., Choi, G., Park, J., Kozuka, C., Sears, D.D., Masuzaki, H., and Kim, J.B. (2013). Macrophage glucose-6-phosphate dehydrogenase stimulates proinflammatory responses with oxidative stress. Mol. Cell Biol. *33*, 2425–2435.

Hawley, J.A., Hargreaves, M., Joyner, M.J., and Zierath, J.R. (2014). Integrative biology of exercise. Cell *159*, 738–749.

Hildebrandt, A.L., Pilegaard, H., and Neufer, P.D. (2003). Differential transcriptional activation of select metabolic genes in response to variations in exercise intensity and duration. Am. J. Physiol. Endocrinol. Metab. *285*, E1021–E1027.

Hoffman, N.J., Parker, B.L., Chaudhuri, R., Fisher-Wellman, K.H., Kleinert, M., Humphrey, S.J., Yang, P., Holliday, M., Trefely, S., Fazakerley, D.J., et al. (2015). Global phosphoproteomic analysis of human skeletal muscle reveals a network of exercise-regulated kinases and AMPK substrates. Cell Metab. *22*, 922–935.

Horie, M., Warabi, E., Komine, S., Oh, S., and Shoda, J. (2015). Cytoprotective role of Nrf2 in electrical pulse stimulated C2C12 myotube. PLoS One *10*, 1–13.

Horn, A., Van Der Meulen, J.H., Defour, A., Hogarth, M., Sreetama, S.C., Reed, A., Scheffer, L., Chandel, N.S., and Jaiswal, J.K. (2017). Mitochondrial redox signaling enables repair of injured skeletal muscle cells. Sci. Signal. *10*, 1–12.

Huang, D.W., Sherman, B.T., and Lempicki, R.A. (2008). Systematic and integrative analysis of large gene lists using DAVID bioinformatics resources. Nat. Protoc. *4*, 44–57.

Inoue, M., Jiang, Y., Barnes, R.H., Tokunaga, M., Martinez-Santibañez, G., Geletka, L., Lumeng, C.N., Buchner, D.A., and Chun, T.-H. (2013). Thrombospondin 1 mediates high-fat diet-induced muscle fibrosis and insulin resistance in male mice. Endocrinology *154*, 4548–4559.

Irrcher, I., and Hood, D.A. (2004). Regulation of Egr-1, SRF, and Sp1 mRNA expression in contracting skeletal muscle cells. J. Appl. Physiol. *97*, 2207–2213.

Jentjens, R., and Jeukendrup, A. (2003). Determinants of post-exercise glycogen synthesis during short-term recovery. Sports Med. *33*, 117–144.

Kawata, K., Hatano, A., Yugi, K., Kubota, H., Sano, T., Fujii, M., Tomizawa, Y., Kokaji, T., Tanaka, K.Y., Uda, S., et al. (2018). Trans-omic analysis reveals selective responses to induced and basal insulin across signaling, transcriptional, and metabolic networks. iScience *7*, 212–229.

Kel, A.E., Gössling, E., Reuter, I., Cheremushkin, E., Kel-Margoulis, O.V., and Wingender, E. (2003). MATCH: a tool for searching transcription factor binding sites in DNA sequences. Nucleic Acids Res. *31*, 3576–3579.

Kinsella, R.J., Kahari, A., Haider, S., Zamora, J., Proctor, G., Spudich, G., Almeida-King, J., Staines, D., Derwent, P., Kerhornou, A., et al. (2011). Ensembl BioMarts: a hub for data retrieval across taxonomic space. Database *2011*, bar030.

Loh, K., Deng, H., Fukushima, A., Cai, X., Boivin, B., Galic, S., Bruce, C., Shields, B.J., Skiba, B., Ooms, L.M., et al. (2009). Reactive oxygen species enhance insulin sensitivity. Cell Metab. *10*, 260–272.

Mahoney, D.J., Safdar, A., Parise, G., Melov, S., Fu, M., MacNeil, L., Kaczor, J., Payne, E.T., and Tarnopolsky, M.A. (2008). Gene expression profiling in human skeletal muscle during recovery from eccentric exercise. Am. J. Physiol. Regul. Integr. Comp. Physiol. *294*, R1901–R1910.

Manabe, Y., Miyatake, S., Takagi, M., Nakamura, M., Okeda, A., Nakano, T., Hirshman, M.F., Goodyear, L.J., and Fujii, N.L. (2012). Characterization of an acute muscle contraction model using cultured C2C12 myotubes. PLoS One *7*, e52592.

Mannerås-Holm, L., Kirchner, H., Björnholm, M., Chibalin, A.V., and Zierath, J.R. (2015). mRNA expression of diacylglycerol kinase isoforms in insulin-sensitive tissues: effects of obesity and insulin resistance. Physiol. Rep. *3*, e12372.

Matsuda, N., Hironaka, K.I., Fujii, M., Wada, T., Kunida, K., Inoue, H., Eto, M., Hoshino, D., Furuichi, Y., Manabe, Y., et al. (2020). Monitoring and mathematical modeling of mitochondrial ATP in myotubes at single-cell level reveals two distinct population with different kinetics. Quant. Biol. 1–10, https://doi.org/10.1007/s40484-020-0211-8.

Matys, V., Kel-Margoulis, O.V., Fricke, E., Liebich, I., Land, S., Barre-Dirrie, A., Reuter, I., Chekmenev, D., Krull, M., Hornischer, K., et al. (2006). TRANSFAC(R) and its module TRANSCompel(R): transcriptional gene regulation in eukaryotes. Nucleic Acids Res. *34*, D108–D110.

McCurdy, C.E., Schenk, S., Holliday, M.J., Philp, A., Houck, J.A., Patsouris, D., MacLean, P.S., Majka, S.M., Klemm, D.J., and Friedman, J.E. (2012). Attenuated Pik3r1 expression prevents insulin resistance and adipose tissue macrophage accumulation in diet-induced obese mice. Diabetes *61*, 2495–2505.

Mina, M., Magi, S., Jurman, G., Itoh, M., Kawaji, H., Lassmann, T., Arner, E., Forrest, A.R.R., Carninci, P., Hayashizaki, Y., et al. (2015). Promoter-level expression clustering identifies time development of transcriptional regulatory cascades initiated by ErbB receptors in breast cancer cells. Sci. Rep. *5*, 11999.

Miyamoto, L., Egawa, T., Oshima, R., Kurogi, E., Tomida, Y., Tsuchiya, K., and Hayashi, T. (2013). AICAR stimulation metabolome widely mimics electrical contraction in isolated rat epitrochlearis muscle. Am. J. Physiol. Cell Physiol. *305*, C1214–C1222.

Neubauer, O., Sabapathy, S., Ashton, K.J., Desbrow, B., Peake, J.M., Lazarus, R., Wessner, B., Cameron-Smith, D., Wagner, K.-H., Haseler, L.J., et al. (2014). Time course-dependent changes in the transcriptome of human skeletal muscle during recovery from endurance exercise: from inflammation to adaptive remodeling. J. Appl. Physiol. *116*, 274–287.

Papa, S., Choy, P.M., and Bubici, C. (2019). The ERK and JNK pathways in the regulation of metabolic reprogramming. Oncogene *38*, 2223–2240.

Parolin, M.L., Chesley, A., Matsos, M.P., Spriet, L.L., Jones, N.L., and Heigenhauser, G.J. (1999). Regulation of skeletal muscle glycogen phosphorylase and PDH during maximal intermittent exercise. Am. J. Physiol. *277*, E890–E900.

Peake, J.M., Tan, S.J., Markworth, J.F., Broadbent, J.A., Skinner, T.L., and Cameron-Smith, D. (2014). Metabolic and hormonal responses to isoenergetic high-intensity interval exercise and continuous moderate-intensity exercise. Am. J. Physiol. Endocrinol. Metab. *307*, E539–E552.

Perry, C.G.R., Heigenhauser, G.J.F., Bonen, A., and Spriet, L.L. (2008). High-intensity aerobic interval training increases fat and carbohydrate metabolic capacities in human skeletal muscle. Appl. Physiol. Nutr. Metab. *33*, 1112–1123.

Perry, C.G.R., Lally, J., Holloway, G.P., Heigenhauser, G.J.F., Bonen, A., and Spriet, L.L. (2010). Repeated transient mRNA bursts precede increases in transcriptional and mitochondrial proteins during training in human skeletal muscle. J. Physiol. *588*, 4795–4810.

Romijn, J.A., Coyle, E.F., Sidossis, L.S., Gastaldelli, A., Horowitz, J.F., Endert, E., and Wolfe, R.R. (1993). Regulation of endogenous fat and carbohydrate metabolism in relation to exercise intensity and duration. Am. J. Physiol. *265*, E380–E391.

Roudier, E., Forn, P., Perry, M.E., and Birot, O. (2012). Murine double minute-2 expression is required for capillary maintenance and exercise-induced angiogenesis in skeletal muscle. FASEB J. *26*, 4530–4539.

Scheler, M., Irmler, M., Lehr, S., Hartwig, S., Staiger, H., Al-Hasani, H., Beckers, J., de Angelis, M.H., Häring, H.-U., Weigert, C., et al. (2013).

Cytokine response of primary human myotubes in an in vitro exercise model. Am. J. Physiol. Cell Physiol. *305*, C877–C886.

Spriet, L.L. (1989). ATP utilization and provision in fast-twitch skeletal muscle during tetanic contractions. Am. J. Physiol. *257*, E595–E605.

Spriet, L.L., Matsos, C.G., and Peters, S.J. (1985). Muscle metabolism and performance in perfused rat hindquarter during heavy exercise. Am. J. Physiol. *248*, C109–18.

Trapnell, C., Pachter, L., and Salzberg, S.L. (2009). TopHat: discovering splice junctions with RNA-Seq. Bioinformatics *25*, 1105–1111.

Trapnell, C., Williams, B.A., Pertea, G., Mortazavi, A., Kwan, G., van Baren, M.J., Salzberg, S.L., Wold, B.J., and Pachter, L. (2010). Transcript assembly and quantification by RNA-Seq reveals unannotated transcripts and isoform switching during cell differentiation. Nat. Biotechnol. *28*, 511–515.

van Loon, L.J.C., Greenhaff, P.L., Constantin-Teodosiu, D., Saris, W.H.M., and Wagenmakers, A.J.M. (2001). The effects of increasing exercise intensity on muscle fuel utilisation in humans. J. Physiol. *536*, 295–304.

Wada, T., Hironaka, K., Wataya, M., Fujii, M., Eto, M., Uda, S., Hoshino, D., Kunida, K., Inoue, H., Kubota, H., et al. (2020). Single-cell information analysis reveals that skeletal muscles incorporate cell-to-cell variability as information not noise. Cell Rep. *32*, 108051.

Wagle, A., Jivraj, S., Garlock, G.L., and Stapleton, S.R. (1998). Insulin regulation of glucose-6-phosphate dehydrogenase gene expression is rapamycin-sensitive and requires phosphatidylinositol 3-kinase. J. Biol. Chem. *273*, 14968–14974.

Wagner, K.R., Kauffman, F.C., and Max, S.R. (1978). The pentose phosphate pathway in regenerating skeletal muscle. Biochem. J. *170*, 17–22.

Wang, L., Davis, S.S., Borch Jensen, M., Rodriguez-Fernandez, I.A., Apaydin, C., Juhasz, G., Gibson, B.W., Schilling, B., Ramanathan, A., Ghaemmaghami, S., et al. (2019). JNK modifies neuronal metabolism to promote proteostasis and longevity. Aging Cell *18*, e12849.

Williamson, D.L., Bolster, D.R., Kimball, S.R., Jefferson, L.S., and David, L. (2006). Time course changes in signaling pathways and protein synthesis in C2 C12 myotubes following AMPK activation by AICAR. Am. J. Physiol. Endocrinol. Metab. *17033*, 80–89.

Wu, C.L., Satomi, Y., and Walsh, K. (2017). RNA-seq and metabolomic analyses of Akt1-mediated muscle growth reveals regulation of regenerative pathways and changes in the muscle secretome. BMC Genomics *18*, 1–18.

Yamasaki, K.I., Hayashi, H., Nishiyama, K., Kobayashi, H., Uto, S., Kondo, H., Hashimoto, S., and Fujisato, T. (2009). Control of myotube contraction using electrical pulse stimulation for bio-actuator. J. Artif. Organs *12*, 131–137.

Yugi, K., Kubota, H., Toyoshima, Y., Noguchi, R., Kawata, K., Komori, Y., Uda, S., Kunida, K., Tomizawa, Y., Funato, Y., et al. (2014). Reconstruction of insulin signal flow from phosphoproteome and metabolome data. Cell Rep. *8*, 1171–1183.

Yugi, K., Kubota, H., Hatano, A., and Kuroda, S. (2016). Trans-omics: how to reconstruct biochemical networks across multiple 'omic' layers. Trends Biotechnol. *34*, 276–290.

iScience, Volume *23*

Supplemental Information

Trans-omic Analysis Reveals ROS-Dependent Pentose Phosphate Pathway Activation after High-Frequency Electrical Stimulation in C2C12 Myotubes

Daisuke Hoshino, Kentaro Kawata, Katsuyuki Kunida, Atsushi Hatano, Katsuyuki Yugi, Takumi Wada, Masashi Fujii, Takanori Sano, Yuki Ito, Yasuro Furuichi, Yasuko Manabe, Yutaka Suzuki, Nobuharu L. Fujii, Tomoyoshi Soga, and Shinya Kuroda

Supplemental Information

Supplemental figures

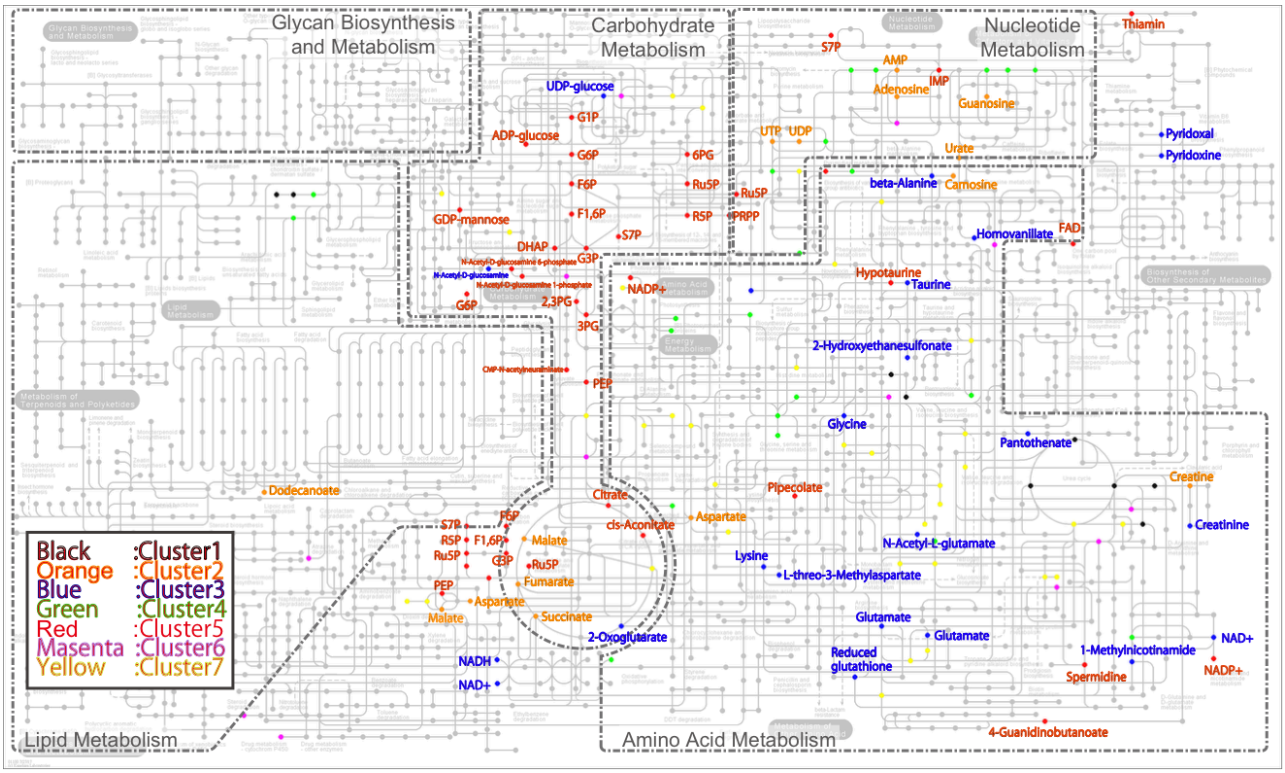

Figure S1 - The measured metabolites in each cluster were mapped on the KEGG global metabolism map. Names colored in orange, blue, and red correspond to metabolites in clusters 2, 3, and 5 in Fig 2, respectively. Related to Figure 2 and 3.

A

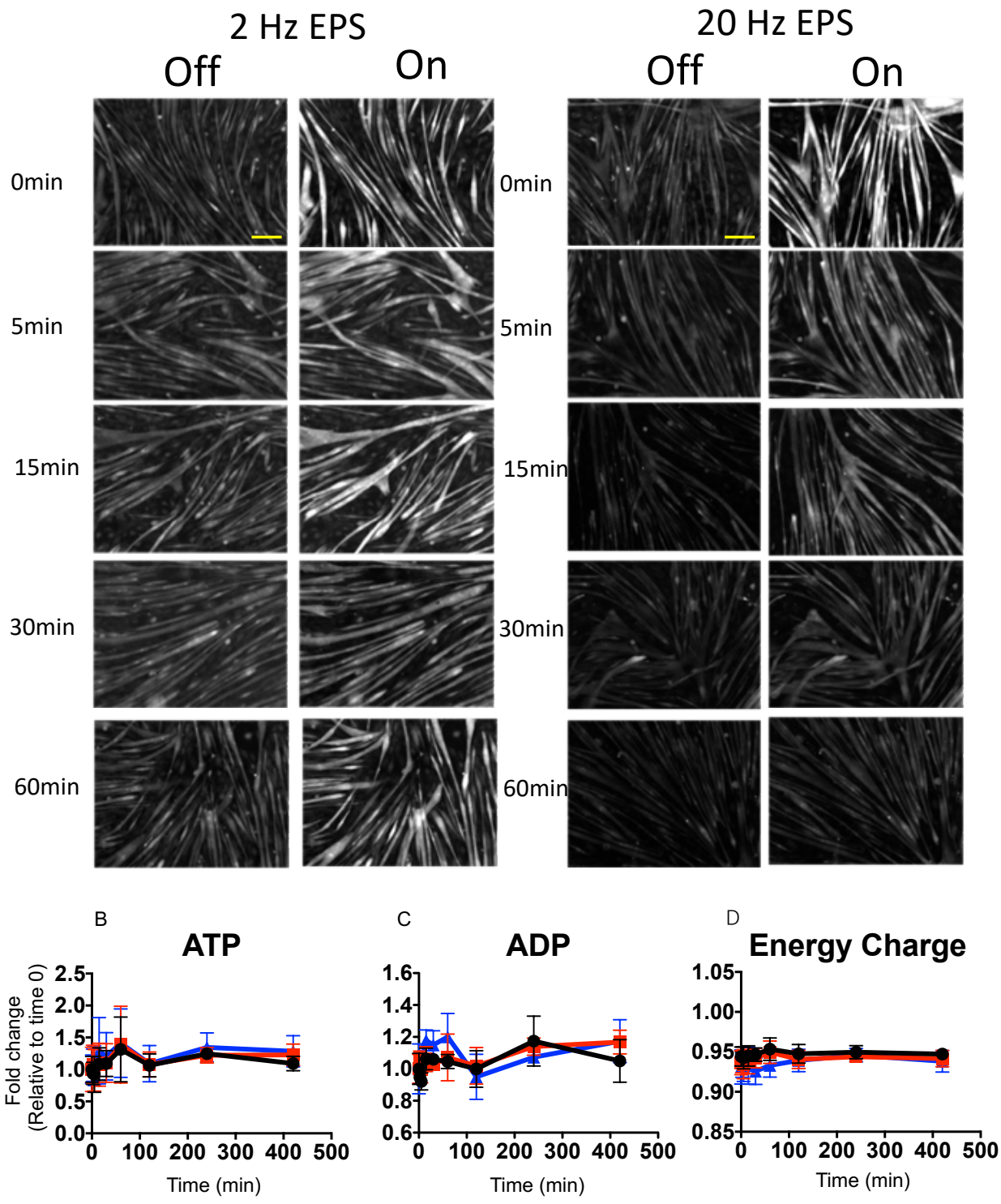

Figure S2 - (A) Images of EPS-induced Ca^{2+} signals in myotubes at 0, 5, 15, 30 and 60 min of 2 Hz or 20 Hz EPS. Scale bar is 150 um. (B) ATP and (C) ADP levels and (D) calculated energy charge ([ATP] + 0.5*[ADP]/[ATP]+[ADP]+[AMP]) during 0, 2 and 20 Hz EPS. Related to Figure 3.

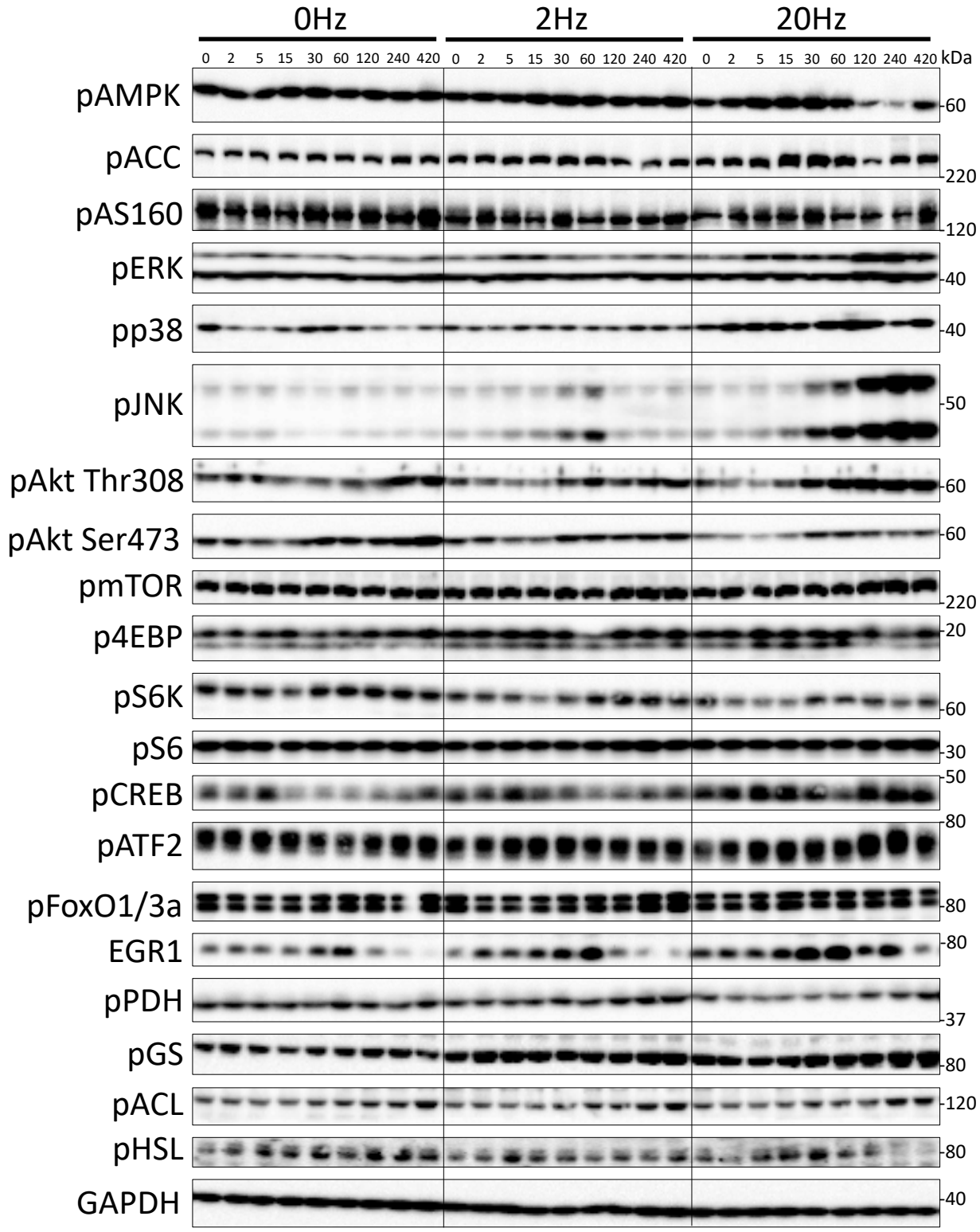

Figure S3 - Representative images of signaling molecules detected by Western blotting. Related to Figure 4.

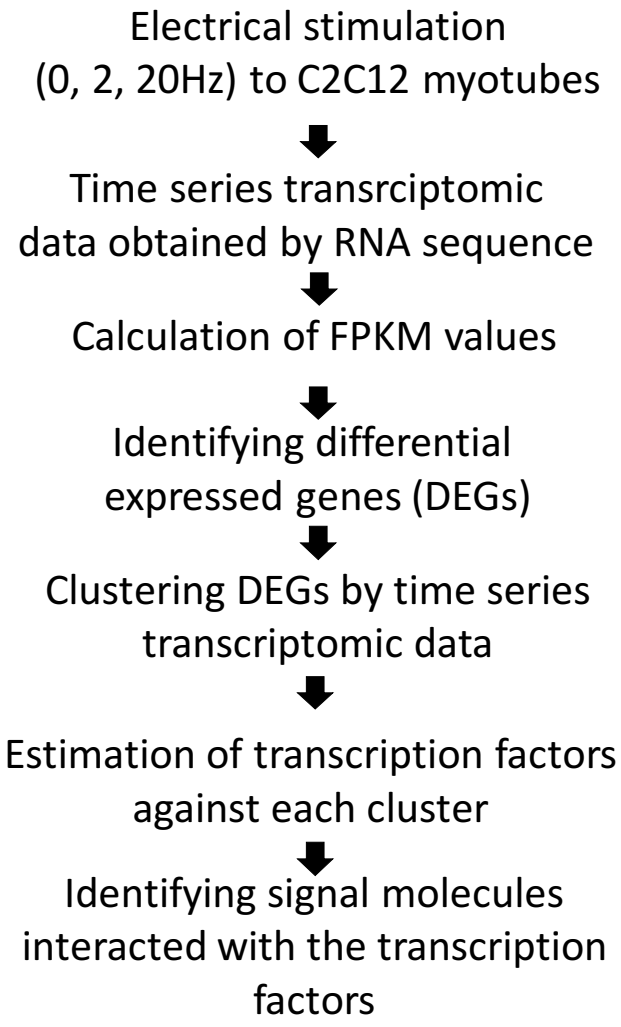

Figure S4 - Analysis of transcriptomic data.

C2C12 myotubes were collected at each time point. RNA sequencing was performed on Hiseq 2500 (Ilumina) (n = 1). Sequencing reads were mapped using TOPHAT v2.0.7, and FPKM values were calculated using Cufflinks. The differentially expressed genes (DEGs) were identified as genes with one or more FPKM values increased or decreased >2.0 fold compared with FPKM at time 0 at 2 Hz or 20 Hz. As a result, 800 genes were identified as DEGs. Hierarchical clustering was performed on these 800 DEGs. TFs were predicted for DEGs in each cluster. Molecules upstream of the predicted TFs were identified as regulators using the KEGG database. Related to Figure 5 and 6.

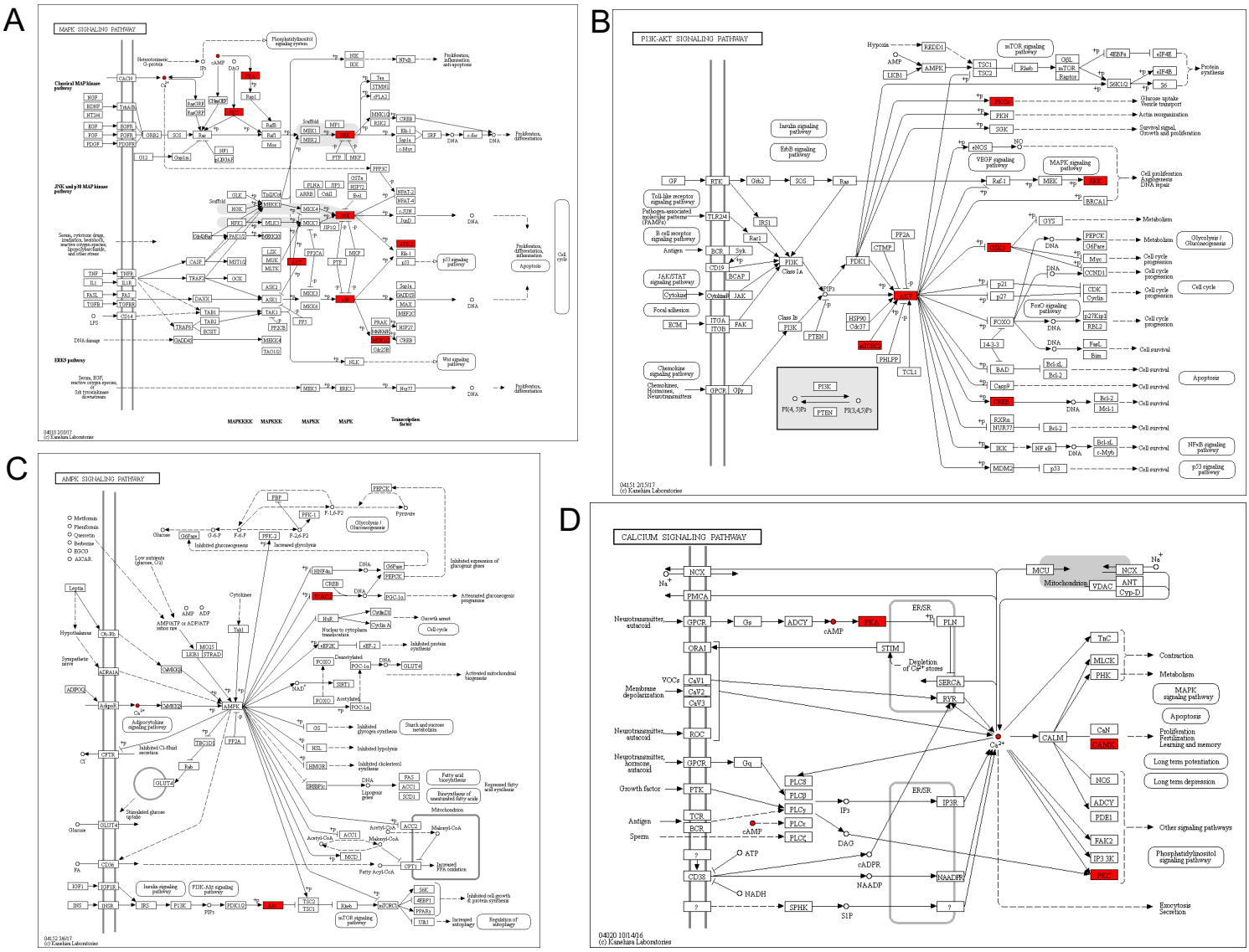

Figure S5 - Identification of regulators upstream of predicted TFs in KEGG signaling pathway map. Related to Figure 6 and 7.

(A) MAPK signaling pathway, (B) PI3-Akt signaling pathway, (C) AMPK signaling pathway, and (D) calcium signaling pathway. Red indicates identified regulators.

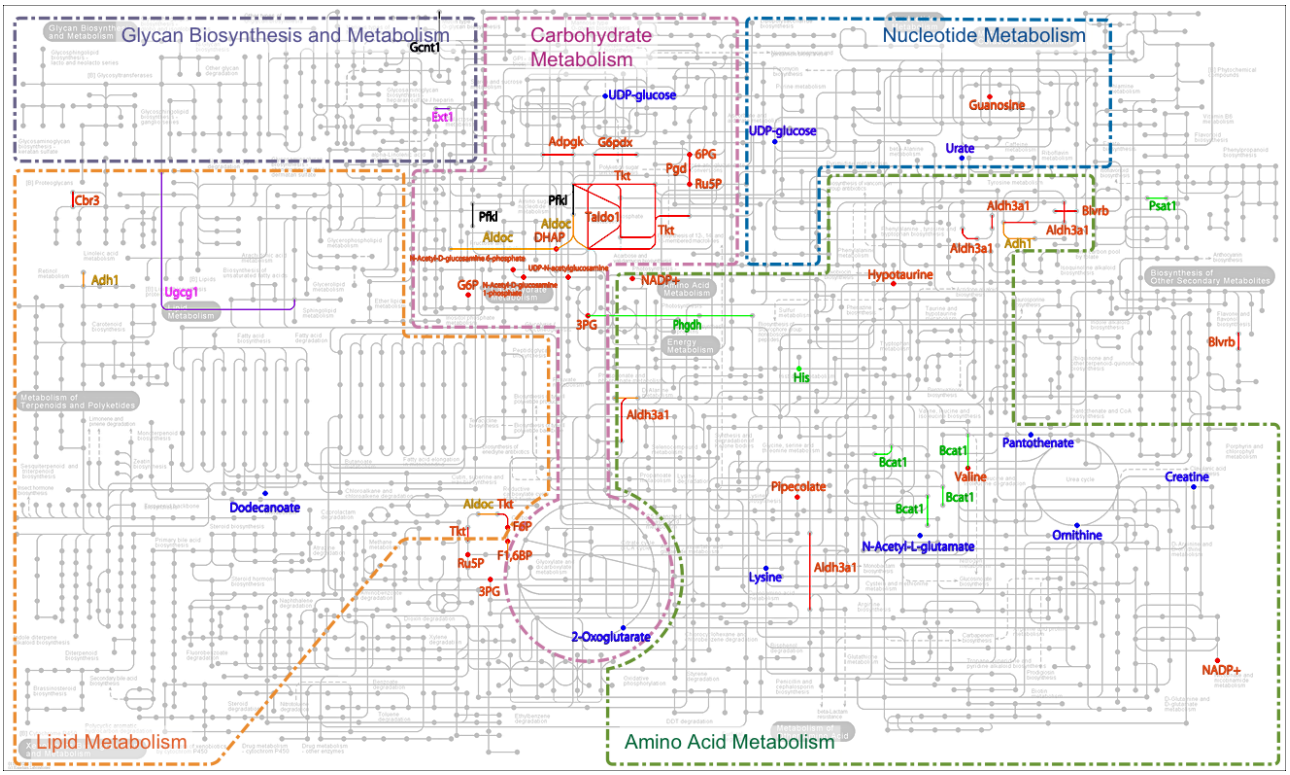

Figure S6 - Identification of significantly changed metabolites and differentially expressed responsible metabolic enzymes. Related to Figure 7.

Red- and blue-colored dots and names indicate metabolites with continuous increase and decrease in levels, respectively. Green-colored dots and names indicate metabolites that both increased and decreased during the time course. Colored lines and names indicate differentially expressed responsible metabolic enzymes in clusters (orange: cluster 1, green: cluster 3, red: cluster 4, blue: cluster 5, purple: cluster 7, black: cluster 8.)

Supplement tables

Table S1. Metabolites in each cluster. Related to Figure 2.

1	2	3	4	5	6	7
Arg	AMP	1-Methylnicotinamide	2-Deoxycytidine	2,3-DPG	1-Methyladenosine	2-Oxoisopentanoate
Argininosuccinate	Adenosine	2-Hydroxyglutarate	4-Acetylbutyrate	2-Hydroxypentanoate	4-Oxopentanoate	2AB
Betaine	Asp	2-Oxoglutarate	5-Methyltetrahydrofolate	3PG	5-Methylthioadenosine	4-Methyl-2-oxopentanoate
Choline	Carnosine	3-Aminoisobutyrate	ADP	5-Aminovalerate	AICAR	5-Oxoproline
Citrulline	Creatine	3-Hydroxy-3-methylglutarate	ATP	6-Phosphogluconate	Adenine	Ala
Glu-Glu	Dodecanoate	3-Methylhistidine	Butanoate	ADP-glucose	Adipate	Asn
Guanidinoacetate	Fumarate	ADMA	CDP-choline	CMP	Allantoin	CDP
N-Acetylleucine	Gly-Leu	Carbamoylaspartate	CTP	CMP-N-acetylneuraminate	Azelate	Dodecanedioate
Phosphorylcholine	Guanosine	Carnitine	Citramalate	Citrate	Citraconate	GABA
	Malate	Creatinine	Cytidine	DHAP	Diethanolamine	Gln
	Pelargonate	Glu	GDP	F1,6P	Glutarate	Gluconate
	Succinate	Glutathione(ox)	GMP	F6P	Glycerate	Glucosamine
	UDP	Glutathione(red)	GTP	FAD	Glycolate	Glucuronate
	UTP	Gly	Hexanoate	G1P	Malonate	Glycerophosphate
	Urate	Gly-Gly	Indole-3-acetate	G3P	Phthalate	His
	beta-Ala-Lys	Glycerophosphorylcholine	N-Methylalanine	G6P	Putrescine(1,4-Butanediamine)	Hydroxyproline
	Pyridoxamine 5-phosphate	Homovanillate	Nicotinamide	GDP-mannose	Terephthalate	Ile
	Proline betaine	Isethionate	O-Phosphoserine	Hypotaurine	UDP-N-acetylglucosamine	Isocitrate
	Methyl sulfate	Lys	SAH	IMP	UDP-glucuronate	Lactate
		N-Acetyl-beta-alanine	Ser	N1-Acetylspermidine	Urea	Leu
		N-Acetylglucosamine	Thymidine	NADP+	o-Acetylcarnitine	Met
		N-Acetylglutamate	UMP	PEP	Acetyl CoA	NADPH
		N-Formylmethionine	Ethanolamine phosphate	PRPP		Ophthalmate
		N-epsilon-Acetyllysine		Pipecolate		Ornithine
		N6,N6,N6-Trimethyllysine		R5P		Phe
		NAD+		Ru5P		Pro
		NADH		S7P		Pyruvate
		Pantothenate		Spermidine		SAM+
		Pyridoxal		Thiamine		Thr
		Pyridoxine		cis-Aconitate		Trp
		S-Lactoylglutathione		gamma-Guanidinobutyrate		Tyr
		Taurine		Ribulose 1,5-diphosphate		Val
		Threonate		N-Acetylglucosamine 1-phosphate		alpha-Aminoadipate
		UDP-glucose		N-Acetylglucosamine 6-phosphate		
		beta-Ala		Methionine sulfoxide		
		gamma-Butyrobetaine				
		glycogen				
		threo-beta-methylaspartate				
		reduced/oxidized glutathione				
		Thiamine monophosphate				

Table S2. Significantly changed metabolites after 20 Hz EPS. Red, blue, and green indicate metabolites that continuously increased, continuously decreased, and both increased and decreased, respectively. Related to Figure 3.

0 Hz vs 2 Hz	0 Hz vs 20 Hz	2 Hz vs 20 Hz
None	G6P	G6P
	F6P	F6P
	F1,6P	F1,6P
	DHAP	DHAP
	3PG	3PG
	2-Oxoglutarate	2-Oxoglutarate
	2-Hydroxyglutarate	2-Hydroxyglutarate
	6-Phosphogluconate	Succinate
	Ru5P	6-Phosphogluconate
	N-Acetyl-beta-alanine	Ru5P
	Urate	N-Acetyl-beta-alanine
	N-Acetylglutamate	Urate
	Dodecanoate	N-Acetylglucosamine 6-phosphate
	Pantothenate	UDP-glucose
	N-Acetylglucosamine 1-phosphate	CMP-N-acetylneuraminate
	N-Acetylglucosamine 6-phosphate	NAD+
	UDP-glucose	Gly
	UDP-N-acetylglucosamine	Ala
	CMP-N-acetylneuraminate	Hypotaurine
	NADP+	5-Aminovalerate
	Hypotaurine	Val
	5-Aminovalerate	Pipecolate
	Val	Ile
	Pipecolate	Gly-Gly
	Creatine	Lys
	Gly-Gly	Methionine sulfoxide
	Ornithine	Phosphorylcholine
	Lys	N6,N6,N6-Trimethyllysine
	His	ADMA
	Methionine sulfoxide	reduced/oxidized glutathione
	Guanosine	
	reduced/oxidized glutathione	

Table S3. Signaling molecules in each cluster. Related to Figure 4.

1	2	3	4
pAkt Ser473	pACL	pAMPK	pp38
pAkt Thr308	pAS160	pACC	pCREB
EGR1	pFoxO1/3a	pHSL	pERK
pGS	pPDH	p4EBP	pATF
pmTOR	pS6K		pJNK
			pS6

Table S4. KEGG pathway analysis of genes enriched in each cluster. Related to Figure 5.

Cluster	Term	Count	P-Value	Benjamini	Genes
1	Fructose and mannose metabolism	2	8.70E-02	8.10E-01	*EGR1, IL6*
	Prion diseases	2	8.20E-02	9.60E-01	*Akr1c13, aldoc*
2	MAPK signaling pathway	6	2.80E-03	1.20E-01	*DDIT3, FOS, DUSP4, DUSP5, Gadd45g, Hspb1*
	p53 signaling pathway	3	2.80E-02	4.80E-01	*Gadd45g, SESN2, mdm2*
3	Glycine, serine and threonine metabolism	3	4.90E-03	1.90E-01	*PHGDH, SHMT2, PSAT1*
	Methane metabolism	2	2.30E-02	2.90E-01	*cat, SHMT2*
	Vitamin B6 metabolism	2	2.00E-02	3.50E-01	*AOX1, PSAT1*
	One carbon pool by folate	2	5.20E-02	4.40E-01	*mthfd2, SHMT2*
4	Glutathione metabolism	10	4.40E-09	4.00E-07	*G6pdx, GCLC, GCLM, gsta1, GSTA4, GSTP1, mgst2, PGD, gstm1, gsr*
	Metabolism of xenobiotics by cytochrome P450	9	6.00E-07	2.70E-05	*adh7, ALDH3A1, CYP1B1, ephX1, gsta1, GSTA4, GSTP1, mgst2, gstm1*
	Drug metabolism	7	1.80E-04	5.50E-03	*adh7, ALDH3A1, gsta1, GSTA4, GSTP1, mgst2, gstm1*
	Pentose phosphate pathway	4	3.00E-03	6.60E-02	*G6pdx, PGD, taldo1, tkt*
	Porphyrin and chlorophyll metabolism	3	4.50E-02	5.70E-01	*BLVRB, FTH1, hmox1*
	Aminoacyl-tRNA biosynthesis	3	8.10E-02	7.20E-01	*AARS, Nars, SARS*
5	Phosphatidylinositol signaling system	3	3.30E-02	9.00E-01	*dgkq, Pik3r1, PIK3C2B*
6	None				
7	Focal adhesion	6	3.30E-03	1.70E-01	*Igf1, Pak3, BCL2, Pdgfb, Thbs1, thbs2*
	Prostate cancer	3	8.00E-02	7.90E-01	*Igf1, BCL2, Pdgfb,*
	TGF-beta signaling pathway	3	7.50E-02	8.90E-01	*INHBA, Thbs1, thbs2,*
8	Cell cycle	8	5.90E-07	2.20E-05	*ttk, BUB1, Cdk1, CCNA2, CCNB2, PTTG1, PLK1, CCNB1*
	Progesterone-mediated oocyte maturation	6	2.20E-05	4.10E-04	*BUB1, Cdk1, CCNA2, CCNB2, PLK1, CCNB1*
	Oocyte meiosis	6	9.30E-05	1.20E-03	*BUB1, Cdk1, CCNB2, PTTG1, PLK1, CCNB1*
	p53 signaling pathway	4	2.80E-03	2.60E-02	*GTSE1, Cdk1, CCNB2, CCNB1*

Table S5. List of differentially changed responsible metabolic enzymes. Cluster numbers are shown in Figure 5. Colors are shown in Figure S6. Related to Figure 5 and 7.

mmu	gene name	cluster number	color
mmu:11522	Adh1	1	orange
mmu:27384	Akr1c13	1	orange
mmu:11676	Aldoc	1	orange
mmu:216188	Aldh1l2	3	green
mmu:12035	Bcat1	3	green
mmu:236539	Phgdh	3	green
mmu:107272	Psat1	3	green
mmu:11529	Adh7	4	red
mmu:72141	Adpgk	4	red
mmu:11670	Aldh3a1	4	red
mmu:233016	Blvrb	4	red
mmu:109857	Cbr3	4	red
mmu:13078	Cyp1b1	4	red
mmu:14381	G6pdx	4	red
mmu:14782	Gsr	4	red
mmu:18104	Nqo1	4	red
mmu:110208	Pgd	4	red
mmu:67103	Ptgr1	4	red
mmu:21351	Taldo1	4	red
mmu:21881	Tkt	4	red
mmu:108155	Ogt	5	blue
mmu:20148	Dhrs3	7	purple
mmu:14042	Ext1	7	purple
mmu:15117	Has2	7	purple
mmu:22234	Ugcg	7	purple
mmu:14537	Gcnt1	8	black
mmu:18641	Pfkl	8	black

Table S6. KEGG pathway analysis of 27 differentially changed responsible metabolic enzymes. Related to Figure 5 and 7.

Rank	Term	number of genes	P-Value	Benjamini
1	Metabolic pathways	18	1.10E-08	4.50E-07
2	Carbon metabolism	9	1.10E-06	2.30E-05
3	Biosynthesis of antibiotics	10	1.50E-06	2.10E-05
4	Pentose phosphate pathway	6	1.20E-05	1.30E-04
5	Biosynthesis of amino acids	7	4.90E-05	4.20E-04
6	Glycolysis / Gluconeogenesis	6	1.00E-04	7.30E-04
7	Metabolism of xenobiotics by cytochrome P450	5	1.00E-02	6.00E-02
8	Retinol metabolism	3	3.40E-02	1.60E-01
9	Tyrosine metabolism	3	3.40E-02	1.60E-01
10	Chemical carcinogenesis	4	6.20E-02	2.60E-01

Table S7. KEGG pathway analysis of the differentially changed responsible metabolic enzymes in cluster 4. Related to Figure 5 and 7.

Rank	Term	number of genes	P-Value	Benjamini
1	Carbon metabolism	5	1.50E-05	1.90E-04
2	Pentose phosphate pathway	4	8.60E-06	2.20E-04
3	Metabolism of xenobiotics by cytochrome P450	4	8.60E-05	7.40E-04
4	Biosynthesis of antibiotics	5	1.60E-04	1.10E-03
5	Metabolic pathways	8	6.00E-04	3.10E-03
6	Glutathione metabolism	3	2.60E-03	1.10E-02
7	Glycolysis / Gluconeogenesis	3	3.80E-03	1.40E-02
8	Chemical carcinogenesis	3	7.20E-03	2.30E-02
9	Tyrosine metabolism	2	5.40E-02	1.50E-01
10	Drug metabolism - cytochrome P450	2	9.00E-02	2.20E-01

Transparent Methods

C2C12 culture

C2C12 myoblasts were seeded into four-well rectangular plates at a density of 3.0×10^5 cells/well, with 3 mL of growth medium comprising Dulbecco's Modified Eagle's Medium (DMEM with 25 mM glucose; Wako, Japan) supplemented with 10% fetal bovine serum. Myoblasts culture was maintained in an incubator at 37°C under a 5% CO_2 atmosphere. After 2 days, the medium was replaced with a differentiation medium consisting of DMEM supplemented with 2% horse serum. Six days after differentiation, cells were used for EPS.

Electrical pulse stimulation (EPS) and N-acetylcysteine (NAC) treatment

EPS was performed using the method of Manabe et al. (Manabe et al., 2012). Briefly, differentiated C2C12 myotubes were used 16 h after the final change of medium. The four-well plates were connected to the electrical stimulation apparatus, a four-well C-Dish (Ion Optix Corp., Milton, MA, USA), and myotubes were stimulated by electric pulses generated by an electrical pulse generator (Uchida Denshi, Hachioji, Japan). Myotubes were stimulated with electric pulses of 50 V at 0, 2, or 20 Hz for 3 ms for a given time period in an incubator at 37°C. We used 2 Hz for low frequency and 20 Hz for high frequency stimulation. Previous studies confirmed that 20 Hz was high frequency for C2C12 myotubes (Fujita et al., 2007; Yamasaki et al., 2009) but 20 Hz is not considered high frequency stimulation for skeletal muscle *in vivo* (Cairns et al., 2007). To inhibit the accumulation of ROS, we added NAC (5 mM) after 1 h of 20 Hz EPS and collected cells 3 h after the EPS.

Metabolome Analysis

The stimulated cells were washed twice with 5% mannitol and incubated for 10 min in 1 mL methanol containing 25 μM each of the three internal standards [L-methionine sulphone (Wako), D-camphor-10-sulphonic acid (Dojindo, Kumamoto, Japan), and 2-(N-morpholin-o)ethanesulfonic acid (Wako)]. After 500 uL Milli-Q purified water was added, 600 uL of the solution was taken and mixed well with 400 uL chloroform and then centrifuged for 15 min at 20,000 g and 4°C. The separated 400 uL aqueous layer was centrifugally filtered through a 5 kDa cutoff filter (Millipore, Burlington, MA, USA) to remove residual protein. The filtrate (320 μL) was lyophilized and dissolved in 50 uL Milli-Q water containing reference compounds [200 μM each of trimesate (Wako) and 3-aminopyrrolidine (Sigma-Aldrich, St. Louis, MO, USA)] and then injected into a CE-TOF-MS system (Agilent Technologies, Santa Clara, CA, USA) (Soga et al., 2006, 2009). We performed independent biological triplicates and excluded metabolites that could not be measured in any of the three samples. For data analysis, the obtained

absolute concentration (μM) in the suspension was normalized to that at time 0 to generate relative values.

Glycogen content assay

Glycogen content was quantified using the method of Noguchi et al. (Noguchi et al., 2013). The cell suspension was incubated for 1 h with 1.2 mL of 30% (w/v) KOH solution at 95°C; 61.2 uL of glacial acetic acid and 1% (w/v) linear polyacrylamide were added to 200 uL of the cell suspension to coprecipitate glycogen. Then 400 uL pure ethanol was added to the mixture to precipitate the total glycogen and the mixture was centrifuged for 15 min at 15,000 r.p.m. at 4°C. The supernatants were discarded, and the pellets were resuspended in 50 uL of 50 mM NaOAc buffer (comprising an equal volume of 50 mM sodium acetate and 50 mM acetate). Then 600 uL pure ethanol was added to the resuspended sample. The resuspended sample was centrifuged for 15 min at 15,000 r.p.m. at 4°C. After the supernatant was discarded, the pellet was dried to eliminate any residual ethanol and incubated with 20 uL amyloglucosidase (0.1 mg/mL in 50 mM NaOAc buffer) for 2 h at 55°C. After the incubation, hydrolyzed glycogen was measured using the glucose assay.

Intracellular calcium ion (Ca^{2+}) measurement

C2C12 myotubes were washed twice with phosphate buffered saline (PBS). Ca^{2+} assay buffer, comprising Fluo-8 dye loading solution (AAT Bioquest Inc., Sunnyvale, CA, USA) and DMEM cell medium without serum, was added to the wells and incubated at 37°C for 30 min. Myotubes were stimulated with electric pulses at 2 Hz or 20 Hz in the incubator and observed at the indicated time under an inverted fluorescence microscope, IX 83 (Olympus, Tokyo, Japan) 755 equipped with a UPLSAPO10X2 objective lens (Olympus) an ORCA-R2 C10600-10B CCD camera (Hamamatsu Photonics, Shizuoka, Japan) , a U-HGLGPS mercury lamp (Molecular Devices, San Jose, CA, USA), a U-FBNA mirror unit (Olympus), an MD XY30100T-META automatically programmable stage position (Molecular Devices.).

Western blotting

Total proteins were extracted from cells by 50 mM Tris-Cl pH 7.5 with 2% SDS at the indicated time points after EPS and subjected to standard SDS-PAGE. The resolved proteins were transferred to nitrocellulose membranes and probed with specific antibodies (antibodies against pAKT [Ser473, #9271, Thr308, #9275], pAMPK [Thr172, #2535], pACC [Ser89, #3661], pAS160 [Thr642, #4288], pERK [Thr202/Tyr204, #9101], pp38 [Thr180/Tyr182, #9211], pS6K [Thr389, #9205], p4EBP [Thr37/46, #2855], pCREB [Ser133, #9198], pJNK [Thr183/Tyr185, #4668], pmTOR [Ser2488, #2971], pATF2

[Thr71, #9221], pACL [Ser455, #4331], pFoxo1/3a [Thr24/Thr32, #9464], pHSL [Ser563, #4139], pGS [Ser641, #3891], EGR1 [#4154], and GAPDH [#2118] were purchased from Cell Signaling Technology Japan (Tokyo, Japan); antibody against pPDH [Ser293, ab92696] was purchased from Abcam (Cambridge, UK). The signal was visualized using chemiluminescence and horseradish peroxidase (HRP)-conjugated secondary antibodies (GE Healthcare, Chicago, IL, USA) and the Immobilon Western Chemiluminescent HRP Substrate (Millipore) using a LAS4000 imager (Fujifilm, Tokyo, Japan). The intensities of the specific bands were quantified using TotalLab TL120 (Nonlinear Dynamics) analysis software. Quantitative values were normalized using GAPDH quantities as standards.

RNA Sequencing

Total RNA was extracted from C2C12 myotubes at 0, 1, 3, and 6 h after 0, 2, or 20 Hz EPS using RNeasy Mini Kit (Qiagen, Hilden, Germany). mRNA was enriched from total RNA using poly(A) selection, and quality of the mRNA samples was validated using 2100 Bioanalyzer (Agilent). RNA integrity number (RIN) values were a range of 8.9-9.7 across samples. Standard Illumina protocols were used to generate 101-base pair, paired-end sequencing reads on the HiSeq 2500 platform (Illumina, San Diego, CA, USA) (Matsumoto et al., 2014). Q30, which is an index of sequence quality, was 86-88% and sequencing depth was more than 50.0 million reads across samples. The sequence data are deposited to DDBJ (Accession number DRA010400).

Identification of differentially expressed genes

The obtained sequencing reads were aligned to the reference mouse genome sequence GRCm38 (Ensemble release 75), using TopHat v2.0.7 (Trapnell et al., 2009). Mapping rate using TOPHAT across samples was 74-79%. FPKM values were calculated using Cufflinks (Trapnell et al., 2010). We removed genes with FPKM < 1 at all time points based on results from a previous RNA-seq study (Väremo et al., 2015). The DEGs were identified as genes with FPKM values that changed more than 2.0-fold and less than 0.5-fold compared with those at time 0 at more than one time point under 2 and/or 20 Hz.

Hierarchical clustering

We performed hierarchical clustering analysis by Ward method using MATLAB (Mathworks) (Sano et al., 2016). For normalization, L2 normalization was performed for each time series data of metabolites, signal molecules, and transcripts.

TF prediction using Motif Enrichment Analysis

We performed motif enrichment analysis following CIDER methods (Mina et al., 2015) to determine enrichment of TF binding motifs in promoter region [−300 bp to +100 bp flanking the consensus transcription start site (Arner et al., 2015; Kinsella et al., 2011)] of DEGs in each cluster. Binding sites of each TF were determined using sequences obtained from Ensembl BioMart (Kinsella et al., 2011), TRANSFAC Pro (Matys et al., 2006), and the Match tool (Kel et al., 2003). We used extended vertebrate_non_redundant_min_SUM.prf, one of the parameter sets prepared in TRANSFAC Pro for the threshold of similarity score calculated by Match. The enrichment of TF binding motifs in the promoter of DEGs in each cluster was determined by Fisher's exact test with FDR following Storey's procedure (Storey et al., 2004). The TFs predicted from the significantly enriched TF binding motifs (FDR < 0.01) were identified as the TFs regulating DEGs in each cluster.

Identification of regulators of TFs

Using the accession numbers from TRANSFAC, we associated the significantly enriched TF binding motifs with TFs using the identifiers obtained from matrix.dat in TRANSFAC Pro. The accession numbers of TFs provided in TRANSFAC Pro are associated with the gene IDs in DATF, EMBL, FLYBASE, MIRBASE, PATHODB, PDB, SMARTDB, SWISSPROT, TRANSCOMPEL, or TRANSPATH. To identify regulators of the TFs, the gene IDs from EMBL, PDB, or SWISSPROT that were associated with the accession numbers of human, mouse, and rat TF were converted to KEGG gene IDs using bioDBnet (https://biodbnet-abcc.ncifcrf.gov/) (Mudunuri et al., 2009). We manually determined the upstream regulators of the TFs from the four signaling pathways (MAPK signaling, PI3K-AKT signaling, calcium signaling, and AMPK signaling) based on KEGG.

Identification of responsible metabolic enzymes that were differentially expressed

To identify responsible metabolic enzymes that were differentially expressed, metabolic enzymes with quantitatively changed metabolites as substrates or products were extracted from KEGG database. Among these metabolic enzymes, those encoded by the DEGs were defined as differentially expressed responsible metabolic enzymes.

KEGG pathway analysis

We used the DAVID tool (https://david.ncifcrf.gov/home.jsp) (Huang et al., 2008, 2009) for KEGG pathway analysis.

Statistical analysis

For identification of quantitatively changed metabolites, comparison of the mean concentration of metabolites under 0, 2, and 20 Hz EPS at each time point was performed using Welch's t-test. P values were adjusted for multiple testing with the Storey's procedure (Storey et al., 2004) using MATLAB (Mathworks) function *mafdr* for time points during (0, 2, 5, 15, 30, and 60 min) and after (120, 240, and 420 min) EPS, and the adjusted p values are shown as q values. When $q < 0.2$ at two or more time points, the metabolite was defined as a quantitatively changed metabolite. Statistical comparison of the level of each molecule among 0, 2, and 20 Hz at each time point was performed using two-way ANOVA. The calculated p value for the electrical stimulation was corrected for multiple testing using the Benjamini–Hochberg method, and $q < 0.1$ was regarded as a significant difference.

Supplemental references

Arner, E., Daub, C.O., Vitting-Seerup, K., Andersson, R., Lilje, B., Drablos, F., Lennartsson, A., Ronnerblad, M., Hrydziuszko, O., Vitezic, M., et al. (2015). Transcribed enhancers lead waves of coordinated transcription in transitioning mammalian cells. Science (80-.). *347*, 1010–1014.

Cairns, S.P., Chin, E.R., and Renaud, J.-M. (2007). Stimulation pulse characteristics and electrode configuration determine site of excitation in isolated mammalian skeletal muscle: implications for fatigue. J. Appl. Physiol. *103*, 359–368.

Fujita, H., Nedachi, T., and Kanzaki, M. (2007). Accelerated de novo sarcomere assembly by electric pulse stimulation in C2C12 myotubes. Exp. Cell Res. *313*, 1853–1865.

Huang, D.W., Sherman, B.T., and Lempicki, R.A. (2008). Systematic and integrative analysis of large gene lists using DAVID bioinformatics resources. Nat. Protoc. *4*, 44–57.

Huang, D.W., Sherman, B.T., and Lempicki, R.A. (2009). Bioinformatics enrichment tools: paths toward the comprehensive functional analysis of large gene lists. Nucleic Acids Res. *37*, 1–13.

Kel, A.E., Gössling, E., Reuter, I., Cheremushkin, E., Kel-Margoulis, O. V, and Wingender, E. (2003). MATCH: A tool for searching transcription factor binding sites in DNA sequences. Nucleic Acids Res. *31*, 3576–3579.

Kinsella, R.J., Kahari, A., Haider, S., Zamora, J., Proctor, G., Spudich, G., Almeida-King, J., Staines, D., Derwent, P., Kerhornou, A., et al. (2011). Ensembl BioMarts: a hub for data retrieval across taxonomic space. Database *2011*, bar030.

Manabe, Y., Miyatake, S., Takagi, M., Nakamura, M., Okeda, A., Nakano, T., Hirshman, M.F., Goodyear, L.J., and Fujii, N.L. (2012). Characterization of an Acute Muscle Contraction Model Using Cultured C2C12 Myotubes. PLoS One *7*. e52592.

Matsumoto, K., Suzuki, A., Wakaguri, H., Sugano, S., and Suzuki, Y. (2014). Construction of mate pair full-length cDNAs libraries and characterization of transcriptional start sites and termination sites. Nucleic Acids Res. *42*, e125–e125.

Matys, V., Kel-Margoulis, O. V., Fricke, E., Liebich, I., Land, S., Barre-Dirrie, A., Reuter, I., Chekmenev, D., Krull, M., Hornischer, K., et al. (2006). TRANSFAC(R) and its module TRANSCompel(R): transcriptional gene regulation in eukaryotes. Nucleic Acids Res. *34*, D108–D110.

Mina, M., Magi, S., Jurman, G., Itoh, M., Kawaji, H., Lassmann, T., Arner, E., Forrest, A.R.R., Carninci, P., Hayashizaki, Y., et al. (2015). Promoter-level expression clustering identifies time development of transcriptional regulatory cascades initiated by ErbB receptors in breast cancer cells. Sci. Rep. *5*, 11999.

Mudunuri, U., Che, A., Yi, M., and Stephens, R.M. (2009). bioDBnet: the biological database network. Bioinformatics *25*, 555–556.

Noguchi, R., Kubota, H., Yugi, K., Toyoshima, Y., Komori, Y., Soga, T., and Kuroda, S. (2013). The selective control of glycolysis, gluconeogenesis and glycogenesis by temporal insulin patterns. Mol. Syst. Biol. *9*, 664.

Sano, T., Kawata, K., Ohno, S., Yugi, K., Kakuda, H., Kubota, H., Uda, S., Fujii, M., Kunida, K., Hoshino, D., et al. (2016). Selective control of up-regulated and down-regulated genes by temporal patterns and doses of insulin. *112*, 1–12.

Soga, T., Baran, R., Suematsu, M., Ueno, Y., Ikeda, S., Sakurakawa, T., Kakazu, Y., Ishikawa, T., Robert, M., Nishioka, T., et al. (2006). Differential metabolomics reveals ophthalmic acid as an oxidative stress biomarker indicating hepatic glutathione consumption. J. Biol. Chem. *281*, 16768–16776.

Soga, T., Igarashi, K., Ito, C., Mizobuchi, K., Zimmermann, H.-P., and Tomita, M. (2009). Metabolomic Profiling of Anionic Metabolites by Capillary Electrophoresis Mass Spectrometry. Anal. Chem. *81*, 6165–6174.

Storey, J.D., Taylor, J.E., and Siegmund, D. (2004). Strong control, conservative point estimation and simultaneous conservative consistency of false discovery rates: a unified approach. J. R. Stat. Soc. Ser. B (Statistical Methodol). *66*, 187–205.

Trapnell, C., Pachter, L., and Salzberg, S.L. (2009). TopHat: discovering splice junctions with RNA-Seq. Bioinformatics *25*, 1105–1111.

Trapnell, C., Williams, B.A., Pertea, G., Mortazavi, A., Kwan, G., van Baren, M.J., Salzberg, S.L., Wold, B.J., and Pachter, L. (2010). Transcript assembly and quantification by RNA-Seq reveals unannotated transcripts and isoform switching during cell differentiation. Nat. Biotechnol. *28*, 511–

515.

Väremo, L., Scheele, C., Broholm, C., Mardinoglu, A., Kampf, C., Asplund, A., Nookaew, I., Uhlén, M., Pedersen, B.K., and Nielsen, J. (2015). Proteome- and Transcriptome-Driven Reconstruction of the Human Myocyte Metabolic Network and Its Use for Identification of Markers for Diabetes. Cell Rep. *11*, 921–933.

Yamasaki, K.I., Hayashi, H., Nishiyama, K., Kobayashi, H., Uto, S., Kondo, H., Hashimoto, S., and Fujisato, T. (2009). Control of myotube contraction using electrical pulse stimulation for bio-actuator. J. Artif. Organs *12*, 131–137.